Sheila Azim Piarali

Licenciada em Bioquímica

Development of process control strategies exploiting knowledge from systems biology: Application to MDCK suspension cells

Dissertação para obtenção do Grau de Mestre em Biotecnologia

Orientador: Dr. Moritz von Stosch, Postdoctoral Researcher, FCT-UNL

Co-orientadores: PD Dr. Yvonne Genzel, Senior Scientist, MPI

Dr. Rui M. Freitas Oliveira, Associate Professor, FCT-UNL

Júri:

Presidente: Dr. Carlos Alberto Gomes Salgueiro

Vogais: Dra. Ana Margarida Palma Teixeira

Dr. Moritz von Stosch

FACULDADE DE CIÊNCIAS E TECNOLOGIA
UNIVERSIDADE NOVA DE LISBOA

Outubro 2015

Development of process control strategies exploiting knowledge from systems biology: Application to MDCK suspension cells

ACKNOWLEDGEMENTS

Choosing Systems Biology as the theme of my Master thesis was indeed a challenge and overcoming it would not have been possible if I did not have Dr. Moritz von Stosch as my supervisor.

I want to thank him for his patience, for his will in seeing others succeed, for his kindness and for believing in me.

Also I would like to thank PD Dr. Yvonne Genzel for integrating me at the Max Planck Institute, for always showing availability and for her wise advices.

To my friend Tiago Costa who spent several hours instructing me, supporting me and giving me strength to continue my work.

To my colleagues, João Ramos and André Guerra for the great company throughout these months.

Finally, I would like to thank my family and João for always being there when I needed.

ABSTRACT

Madine Darby Canine Kidney (MDCK) cell lines have been extensively evaluated for their potential as host cells for influenza vaccine production. Recent studies allowed the cultivation of these cells in a fully defined medium and in suspension. However, reaching high cell densities in animal cell cultures still remains a challenge.

To address this shortcoming, a combined methodology allied with knowledge from systems biology was reported to study the impact of the cell environment on the flux distribution. An optimization of the medium composition was proposed for both a batch and a continuous system in order to reach higher cell densities. To obtain insight into the metabolic activity of these cells, a detailed metabolic model previously developed by Wahl A. et. al was used. The experimental data of four cultivations of MDCK suspension cells, grown under different conditions and used in this work came from the Max Planck Institute, Magdeburg, Germany.

Classical metabolic flux analysis (MFA) was used to estimate the intracellular flux distribution of each cultivation and then combined with partial least squares (PLS) method to establish a link between the estimated metabolic state and the cell environment. The validation of the MFA model was made and its consistency checked. The resulted PLS model explained almost 70% of the variance present in the flux distribution.

The medium optimization for the continuous system and for the batch system resulted in higher biomass growth rates than the ones obtained experimentally, 0.034 h^{-1} and 0.030 h^{-1}, respectively, thus reducing in almost 10 hours the duplication time. Additionally, the optimal medium obtained for the continuous system almost did not consider pyruvate.

Overall the proposed methodology seems to be effective and both proposed medium optimizations seem to be promising to reach high cell densities.

RESUMO

Nos últimos tempos, o uso de linhas celulares de Madine Darby Canine Kidney (MDCK) em culturas de células animais tem sido extensivamente explorado devido ao seu potencial como células hospedeiras para a produção de vacinas contra a gripe. Estudos recentes permitiram o cultivo destas células num meio totalmente definido e em suspensão. No entanto, um dos desafios que se mantém é o de atingir elevadas densidades celulares.

De maneira a ultrapassar esta barreira, procedeu-se a uma combinação de metodologias e a conhecimentos de biologia de sistemas de modo a estudar-se o impacto do ambiente da célula nos fluxos intracelulares. Duas otimizações de meios de cultura foram propostas, quer para um sistema contínuo quer para um sistema descontínuo, a fim de se alcançarem densidades celulares mais elevadas.

Para obter um conhecimento mais detalhado sobre a atividade metabólica das células, o presente estudo baseou-se num modelo metabólico desenvolvido por Wahl et. al. Os dados experimentais de quatro culturas de células de MDCK em suspensão foram fornecidos pelo Max Plank Institute, Magdeburgo, Alemanha.

Metabolic flux analysis (MFA) foi utilizado para estimar os fluxos intracelulares e, posteriormente combinado com o *Partial least squares (PLS)* para estabelecer uma ligação entre o estado metabólico estimado e o ambiente extracelular da célula. A validação do modelo de MFA foi feita bem como a análise da sua consistência. O modelo de PLS resultou na explicação de cerca de 70% de variância para a distribuição de fluxos intracelulares.

Ambas as otimizações resultaram em taxas de crescimento mais elevadas que as obtidas experimentalmente, reduzindo em cerca de 10h o tempo de duplicação. A otimização para o sistema contínuo resultou ainda num meio sem piruvato.

Em geral, a metodologia proposta parece ser eficaz e ambas as otimizações indicam ser promissores para alcançar elevadas densidades celulares.

CONTENTS

LIST OF FIGURES

LIST OF TABLES

ACRONYMS

MDCK – Madine Darby Canine Kidney

MFA – Metabolic Flux Analysis

PLS – Partial Least Squares

Gln - Glutamine

NH3 - Ammonia

Glc - Glucose

Lac- Lactate

Glu- Glutamate

Pyr - Pyruvate

Arg - Arginine

Asn - Asparagine

Ala - Alanine

Thr - Threonine

Gly - Glycine

Val - Valine

Ser - Serine

Pro - Proline

Ile - Isoleucine

Leu - Leucine

Met - Methionine

His - Histidine

Phe - Phenylalanine

Asp - Aspartate

Cys - Cysteine

Tyr - Tyrosine

Trp – Tryptophan

TCA – Tricarboxylic acid

ATP – Adenosine triphosphate

DNA – Deoxyribonucleic acid

RNA – Ribonucleic acid

WLS – Weighted Least Squares

LV – Latent variables

X – Independent variables

Y – Dependent variables

T – Scores for the independent variables

U – Scores for the dependent variables

W – Loadings for the independent variables

Q – Scores for the dependent variables

B – Regression coefficient matrix

C1 – Cultivation 1

C2 – Cultivation 2

C3 – Cultivation 3

C4 – Cultivation 4

PPP – Pentose phosphate pathway

Introduction

Influenza constitutes a serious threat to public health. According to sources [1-4], seasonal influenza epidemics affect between 5 and 15% of the world population causing cases of severe illness and about 500.000 deaths every year. The probability that a pandemic influenza outbreak occurs and the concern that comes with it, has led to intensive efforts in the scientific community to increase the production of influenza vaccines [5-7].

Although many alternatives have been developed to control diseases caused by the influenza virus, vaccination remains the most effective prevention strategy [3, 5, 8]. However, antigenic shifts of the virus occur frequently, wherefore new vaccines are needed every season [3, 9]. It takes 3-4 months to prepare a suitable vaccine if a high seed virus is available, whereas the pandemic only takes approximately 3 months for spreading through all continents [6]. Therefore, the development of the vaccine manufacturing process must yield a fast process, which ensures constant high-quality in large quantities.

The traditional approach to produce vaccines against influenza virus uses embryonated chicken eggs [3, 5, 6, 8, 10]. This approach presents considerable drawbacks [11]. For instance, several months are needed to produce chicken flocks capable of producing embryonated eggs. Different studies have also shown that the composition of hemagglutinin changes when the virus is passed to the chicken eggs, leading to: 1) undesired immune responses; 2) the need of an extensive manufacturing control throughout the process due to the inherent microbial burden in eggs; and 3) the difficulties associated with the scale-up processing in a short period of time [4, 8, 12].

Over the past years, a main focus consisted in developing cell culture systems for influenza virus replication. Many cell lines, like African Green Monkey (Vero) and Madine Darby Canine Kidney (MDCK) cells, have been proposed as host cells for influenza vaccine production. Both of these mammalian cell lines can yield high virus titers, show good reproduction of influenza strains and similar characteristics [3, 5, 11-13].

In this study, we focus on MDCK cells. MDCK cells can grow in suspension, which brings more benefits in terms of production costs when compared to adherent cells, due to the elimination of complex processing steps associated with microcarriers [8, 14]. Additionally, these cells have been reported to grow on chemically defined culture media, which diminishes batch-to-batch variations and the risk of contaminations. MDCK cells are also resistant to the toxic effects of trypsin supplementation and, as described before, they are highly permissive for propagation of influenza viruses [1, 7, 10, 11, 15].

During MDCK cultivations, four characteristic process phases are distinguished, namely adaptation phase, exponential growth phase, inhibition phase and confluent phase. During the adaptation or “lag” phase cells are not growing because they are adapting to the culture conditions. In the exponential growth phase the cells grow at maximum specific growth rate. The inhibition phase results in the decrease of the specific growth rate and finally in the confluent phase the specific growth rate approaches to zero due to the lack of nutrients [16].

The infection stage is done towards the end of the exponential phase, because it is where the highest increase in cell concentration occurs and the highest cell density

(number of cells per unit volume) is observed. The infected cells start to produce virus particles, which first accumulate inside the cells and then start budding from the host cells. The released virions then infect other cells, which have been uninfected to this stage. The produced virus can then be separated from the cells/culture by chromatography [2, 13, 17].

Despite having a cell line that can grow in suspension and the respective techniques to isolate the virus, infect the host cells and collect the final product, one of the main challenges that still remains is to ensure high influenza yields and good quality in a short period of time.

One way to overcome this problem is to increase the yield in high cell density cultures. As mentioned before, cell density represents the number of cells per unit volume. In theory, the higher the cell density, the higher the amount of cells per unit volume, therefore more cells are available to be infected at time of infection leading to high virus titers in less time. Distinct strategies are used to reach high cell densities such as genetic modifications of the host cells, improvement of the medium composition and control and analysis of the process [18].

Notwithstanding the existing strategies there are problems that appear when in high cell density conditions that still remain unsolved. For example, it has been observed that from a certain density, the cells start to slow down their growth even though a high number of cells is present in the culture, the so called high cell density effect which was also reported for insect cell lines [6, 19, 20]. In this scenario, specific rates of glucose and glutamine consumption decrease significantly and also apoptosis occurs [9]. It is assumed by many that this effect is due to depletion of nutrients; accumulation of toxic compounds; cell-to-cell contact [18, 21]. Yet, what actually causes it still is not completely known.

Optimization of medium composition and process conditions are some of the strategies used to try to solve these inconveniences. This optimization is often made by trial-and-error processes and by new configurations and modifications of bioreactors [22]. For instance, different process strategies, such as fed-batch or perfusion cultivations, can be used to prevent the occurrence of the high-cell density effect [6, 23]. Albeit, considerable time, equipment and reagents have to be used, in order to achieve the optimal conditions, augmenting the whole process costs and more importantly development time [24].

For these reasons, our goal is to develop an optimization strategy that can:

1) Reduce costs, time and equipment needed;
2) Sustain growth of MDCK suspension cells to high cell densities without affecting the specific productivity of the cells;
3) Yield a fast process, ensuring constant high-quality in large quantities.

The idea behind our study is that the extracellular environment of a cell has an impact on the cell regulation and such on the intracellular flux distribution. Using knowledge from systems biology one could study the importance of the medium composition towards an increase in the biomass growth rate.

To do so, mathematical modelling, an approach used by systems biology is going to be explored [25]. Mathematical models allow the description of the dynamics of the system in study. Based on these models, one can predict the system's behavior at any time and also to obtain quantitative knowledge about the importance of different factors and the range of values in which they are important to improve yield in vaccine production processes [17, 26].

These models can be unstructured and structured. In the first case, intracellular phenomena is not considered whereas in the second case many assumptions are made so that the model looks as realistic as possible. We will focus on structured models. These try to have as much features as they can, different state variables are used to model the system's behavior in different cellular compartments. This means that for each part of the system, the functional mechanism is comprehended and structural connectivity is analyzed [17, 26].

In this particular case, several modelling studies have been made to capture the dynamics of influenza infections [26]. Most these studies focus on the metabolism and growth of the host cell and also the metabolism and kinetics of the influenza infection cycle. The aim of these models is to understand the interactions between the viruses and the host cells and to determine, which parameters impact the most on virus yields.

The model used in this work was based on the metabolic network developed by Wahl et all. It was constructed based on annotated sequences of Canis familiaris, genome databases, metabolic reconstruction and augmented by physiological data reported in literature and obtained experimentally. This model takes two compartments into account, cytosol and mitochondria, as well as transport reactions [16]

Herein, our goal is to sustain growth of MDCK cells to high cell densities by optimizing the medium composition, both for a batch and a continuous system. Besides the mathematical model, two methods are going to be explored. The first one, Metabolic Flux Analysis (MFA) is going to be used to estimate the cell's fluxome and the second one, Partial Least Squares (PLS) will be used to find a regression model between the medium concentrations and the cell's fluxome, in particular focusing on the biomass growth rate.

Materials and Methods

The data of four cultivations of MDCK suspension cells, grown under different conditions and used in this work came from the Max Planck Institute, Magdeburg, Germany.

Table 1. Cultivations considered for MFA and PLS modeling

Cultivation	1	2	3	4
Bioreactor	Stirred-tank	Stirred-tank	Stirred-tank	Wave
Cell line	MDCK.SUS1	MDCK.SUS1	MDCK.SUS2	MDCK.SUS1
Medium growth	SMIF8*	SMIF8*	SMIF8*	SMIF8*
Influenza Strain	A/PR/8/34 (H1N1, RKI)	A/Wisconsin	B/ Malaysia	A/PR/8/34 (H1N1, RKI)

* (protein- and peptide-free, chemically defined medium available from Gibco by contact through K. Scharfenberg, FH Emden/Leer, Germany).

For each cultivation data for the biomass, substrates, products, time points and standard deviations were given. Cell numbers in suspension were determined by trypan blue dye exclusion method with ViCell XR Cell Counter from Beckman Coulter. Concentrations of glucose, lactate, glutamine, glutamate and ammonia in the supernatant were measured by Bioprofile 100 plus from IUL instruments. The concentrations of amino acids were measured using anion exchange chromatography (Dionex AAS equipment).

Treatment and Data Analysis

The first step consisted in making a functional representation of the concentration data using cubic smoothing splines.

Cubic smoothing splines are a form of interpolation where the interpolant is a piecewise polynomial called spline [27, 28]. As they are described by several polynomials, they can make a more realistic description of the data and avoid Runge's phenomenon, an oscillation problem that occurs at the edges of an interval when using polynomial interpolation with polynomials with high degree [29]. For that reason, spline interpolations are preferred over polynomial interpolations.

The spline function (1) has a smoothing parameter, p, that can be chosen from the interval [0 – 1] and depending on its value it describes the data more roughly (p=0) (because the objective function for parameter identification contains the second derivative $D^2 f$ as a regulation term), or it can act as a 'natural' cubic spline interpolant (p=1), describing the data with oscillations that contain inherent noise [27-29]. The goal is to obtain smooth functions that rather describe the true underlying behavior than noise. In principle the function should have a low curvature meaning that the curve should be as monotonic as it can be.

The objective function for parameter identification of the smoothing spline reads,

$$p\sum_{j=1}^{n} w(j)|C_i(j) - f\big(t(j)\big)|^2 + (1-p)\int \beta(x)|D^2 f(x)|^2 \; dx \quad (1)$$

where j = [1, …, n] is the number of points at which concentration data are available; C_i represents the experimental data for each concentration; w is the weight of each point C_i,j, the default value for the weight is one; t represents the time of each entry j; β is the piecewise constant weight function; $D^2 f$ denotes the second derivative of f.

The following table contains the smoothing parameters, p, attributed to each compound for each cultivation when applying cubic smoothing splines.

Table 2. Smoothing parameters attributed for each compound present on each cultivation

	C1	C2	C3	C4
Gln	0	0	0	0
NH_3	0.01	0	0	0.001
Glc	0.1	0	0	0.1
Lac	0.1	0	0	0.01
Glu	0.1	0.1	0.01	0.1
Pyr	0.001	0.001	0.001	0.001
Arg	0.01	0.01	0.001	0.01
Asn	0	0.01	0.001	0
Ala	0	0.01	0.01	0
Thr	0.01	0.1	0.01	0.01
Gly	0	0.01	0.01	0
Val	0	0	0.001	0
Ser	0.01	0.01	0	0.01
Pro	0.1	0.01	0	0
Ile	0	0.01	0	0
Leu	0.001	0.01	0.01	0.001
Met	0	0	0	0
His	0.001	0	0	0
Phe	0	0	0.01	0
Asp	0	0.001	0	0
Cys	0.01	0	0	0.01
Tyr	0.01	0	0.001	0
Trp	0.01	0	0	0

Parameter estimation was made by using an algorithm (csaps; MATLAB, the Mathworks, 2013).

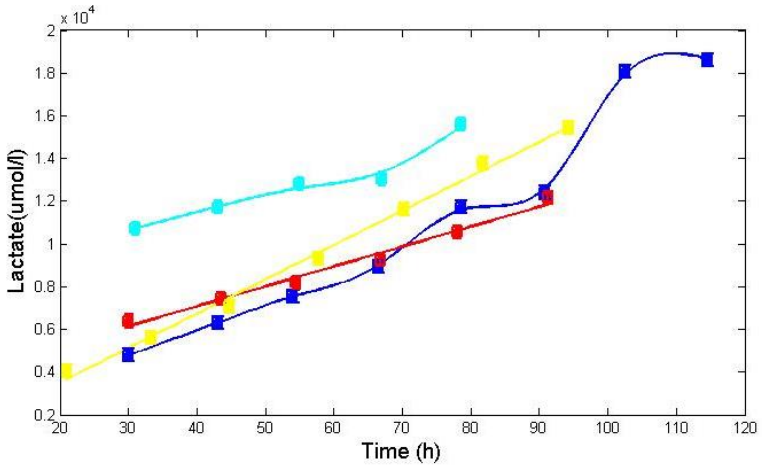

Figure 1. Concentration profiles over time for Lactate excretion during the exponential phase. The solid lines represent the model fit. The first cultivation is represented by dark blue, the second cultivation is represented by red, the third cultivation is represented by yellow and the fourth cultivation is represented by light blue.

Figure 1 serves to explain how this ascription was made. Whenever a compound showed linear behavior the *p* value attributed was equal to zero, as it is demonstrated by the second and third cultivations (red and yellow). The more oscillations a compound showed the greater the *p* value. In the first cultivation (dark blue), lactate showed more oscillation, therefore a *p* value equal to 0.1 was assigned, whereas in the fourth cultivation (light blue) since the oscillation was smoother, a *p* value equal to 0.01 was given. Following this criteria the smoothing parameters were appointed.

When applying this type of interpolation, the concentrations of the experimental data start to depend not only from time but also from the smoothing parameter (2). As our approach is a differential one, the functions obtained for each concentration with the spline interpolation were differentiated over time (3), and using material balance equations, the extracellular rates, $v(t)$ were calculated (4 -5),

$$c = f(t,p) \quad (2)$$

$$\frac{dc}{dt} = \frac{df(t,p)}{dt} \quad (3)$$

$$-\frac{dc}{dt} = v * X_v \quad (4)$$

$$-\frac{dc}{dt} * \frac{1}{X_v} = -\frac{df(t,p)}{dt} * \frac{1}{X_v} = v(t) \quad (5)$$

where X_v is the viable cell concentration.

Note that, in the case of ammonia (6) and glutamine (7), different material balance equations had to be considered because it is known that a spontaneous

decomposition has influence on the formation or/and consumption of the compounds [30, 31]. The considered equations were,

$$\left(-\frac{\mathrm{dfammonia(t,p)}}{\mathrm{d}t}+k*[ammonia]\right)*\frac{1}{Xv}=v_{ammonia}(t)\quad(6)$$

$$\left(-\frac{\mathrm{dfGln(t,p)}}{\mathrm{d}t}-k*[Gln]\right)*\frac{1}{Xv}=\ v_{Gln}(t)\quad(7)$$

Metabolic Flux Analysis (MFA)

MFA: Calculation of the intracellular flux distributions

MFA is a constraint based mathematical method that permits to quantify intracellular fluxes if enough measured fluxes are calculated and given a metabolic network. The following assumptions are based on general MFA theory [32-35].

As mentioned before, the metabolic network used was developed by Wahl et. all [16]. The metabolic pathways considered were glycolysis, the pentose phosphate pathway, the TCA cycle, the glyoxylate shunt, cellular respiration, biosynthesis, the degradation of amino acids, the biosynthesis of biomass and an ATP consumption reaction. Two mechanisms of membrane transport were taken into account. The first between the extracellular medium and the cytoplasm and the second between the cytoplasm and the mitochondria. The biomass components considered were proteins, lipids, DNA, RNA and carbohydrates. The biomass composition was determined from experimental data and from literature [16].

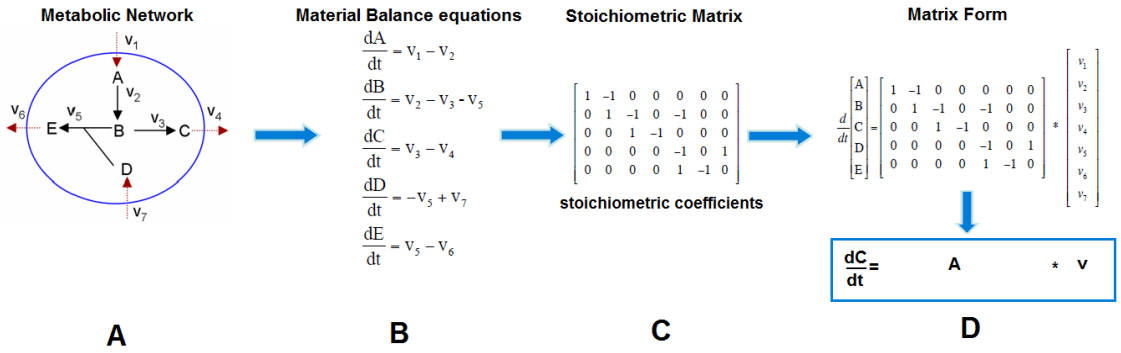

Figure 2. Schematic representation of Metabolic Flux Analysis first steps to calculate intracellular fluxes. (A) Development of a metabolic network of a certain system, (B) Formulation of the respective material balance equations for each metabolite present in the model, (C) Creation of a stoichiometric matrix based on stoichiometric coefficients, (D) Representation of the resulting data into a matrix form.

The metabolic stoichiometric matrix is obtained from the intracellular material balance equations, derived for each metabolite. The stoichiometric matrix comprises the stoichiometric coefficients for the representation of the reactions and for the transport rates. The resulting equations obtained from mass balances over each metabolite are represented in matrix notation by,

$$\frac{dc}{dt} = A * v - \mu * c \text{ (8)}$$

where *A* is an *n x m* matrix of stoichiometric coefficients, *v* an m-dimensional flux vector, μ is the specific growth rate (h^{-1}) and *c* is the concentration of each metabolite (µmol/L) (Figure 2).

It is assumed that the intracellular concentrations of the different metabolites rapidly adjust to new levels, even if a perturbation is observed in the extracellular environment by the cells, wherefore quasi-steady state can be assumed [36]. This means that there is no metabolite accumulation over time. Also the fluxes *v* are usually much greater than the product μ*c*, wherefore the latter term can be dropped and so equation (8) turns into,

$$0 = A * v \text{ (9)}$$

The system can be separated into measured and unmeasured fluxes to,

$$0 = A_k * v_k + A_u * v_u \text{ (10)}$$

where the first term in the right side represents the known part (which includes the measured fluxes, v_k) and the second term in the right side represents the unknown part (which includes the intracellular fluxes, v_u).

Since the metabolic model comprises 134 reactions and has 71 metabolites, at least 63 fluxes (degrees of freedom) needed to be measured to yield a determined system. In such case, the equation to calculate the intracellular fluxes, v_u, would be,

$$v_u = -A_u^{-1} * A_k * v_k \text{ (11)}$$

However, after some considerations, 21 fluxes were set to zero based on assumptions made by Sidorenko et al. [13], another 11 fluxes were set to zero based on the metabolism of amino acids and because no data regarding virus production was considered, other 14 fluxes were set to zero. Additionally, 24 extracellular fluxes were calculated from the experimental data. So in total 70 fluxes, v_k, were considered.

As described by Klamt et al [37], the system can then be classified based on the number of measured fluxes in terms of determinacy and redundancy,

- Undetermined if rank(A_u) < number of v_u, where there are not enough linearly independent constraints for computing all rates of v_u uniquely;
- Determined if rank(A_u) ≥ number of v_u, where there are enough linearly independent constraints for computing all rates of v_u uniquely;
- Redundant if rank(A_u) < m;
- Not redundant if rank(A_u) = m, with m equal to the number of metabolites present in the metabolic network.

In this case, as there are more measured fluxes than degrees of freedom, and consequently there are more equations available than the minimum needed for determinations of the unknown fluxes the system can be classified as determined and redundant and instead of using equation (11), Moore-Penrose pseudo-inverse matrix was used to solve the system,

$$v_u = -A_u^{\#} * A_k * v_k \text{ (12)}$$

MFA: Data accuracy

After the unknown fluxes were calculated, the accuracy of both known and unknown fluxes was checked using redundant measurements, *R*. If the system assumed that the biochemistry behind the metabolic model was correct and there were no errors in the measurements one should verify,

$$0 = R * v_k \quad (13)$$

where,

$$R = A_k - A_u * A_u^{\#} * A_k \quad (14)$$

However, it is most common that experimental data sets present noise or/and in some cases, systematic errors. So equation (13) can be transformed to,

$$e = R_{red} * v_k \quad (15)$$

where R_{red} is the reduced redundancy matrix containing only the independent rows of *R*. With this equation one could then analyze the magnitude of the errors of the data set.

MFA: Data consistency

To evaluate the consistency of the data and model, the consistency index, *h* (16) was calculated,

$$h = e^T * Y^{-1} * \mathrm{e} \quad (16)$$

where,

$$Y = R_{red} * Y_b * {R_{red}}^T \quad (17)$$

For that, Monte Carlo method was applied to generate 1000 data matrices based on the standard deviations of the experimental data. This procedure gave an approximation of the correct variance-covariance matrix, Y_b which was assumed to be diagonal meaning that the measurements are uncorrelated. Monte Carlo simulations are important tools when it comes to estimate model parameters and to perform sensitivity analysis [38].

It is known that when the measurements are uncorrelated, the consistency index is χ^2 distributed [26].

The comparison between *h* and the χ^2 test function provides an idea of how consistent is the experimental data with the assumed biochemistry. For this, reduced redundancy measurements were used as the degrees of freedom for statistical hypothesis testing at a 95% confidence level.

Consistent results should obey this condition $h < \chi^2$. If at a high confidence level one obtains a consistency index greater than the value of the χ^2 distribution, than there is a problem with our data and results should not considered to be reliable [20, 26, 31] .

MFA: Data reconciliation

Finally, to obtain a better estimation for both known and unknown fluxes, Weighted Least Squares (WLS) method was applied according to the following equations,

$$v_{k,corr} = (I - Y_b * R_{red} * (R * Y_b * R_{red})^{-1} * R) * v_k \quad (18)$$

$$v_{u,corr} = -A_u^{\#} * A_k * v_{k,corr} \quad (19)$$

where I is the identity matrix.

Partial Least Squares (PLS)

PLS: Overview

With both extracellular concentrations and cell's fluxome calculated with material balance equations and MFA, respectively, the PLS method was applied to verify how these two variables relate with each other and also to determine the optimal concentrations to reach a high biomass growth rate for both a batch and a continuous system.

PLS is a statistical regression technique highly suited for analyzing high-dimensional data [39].

It differs from conventional regression methods because besides being able to analyze data with many noise, it can efficiently examine the structural relationship between independent variables, X, and dependent variables, Y even when there are more variables in X than (independent) observations [40-43]. This feature is of most interest since the goal of this work is to understand the impact of the medium concentrations (independent variables) on the flux distribution (dependent variables).

Usually, the dependent variables are difficult to obtain or because the techniques used are time-consuming or because they are expensive, whereas independent variables are easy and cheap to obtain [39].

PLS has the particularity of making a regression model so that in the future only independent variables are needed to predict the dependent variables, turning this method into a valuable tool.

PLS regression starts by finding a set of linear combinations, called latent variables (LV), that simultaneously decompose both X and Y with the restriction that these latent variables have the best predictive power as they explain as much as possible the covariance between X and Y. This decomposition results into score matrices, T and U, and loading matrices, W and Q, for X and Y respectively. Using the scores of both variables, the regression coefficient matrix, B, is calculated. Then, new predictions of Y can be made solely by multiplying the B matrix with new X sets (Figure 3) [39-47].

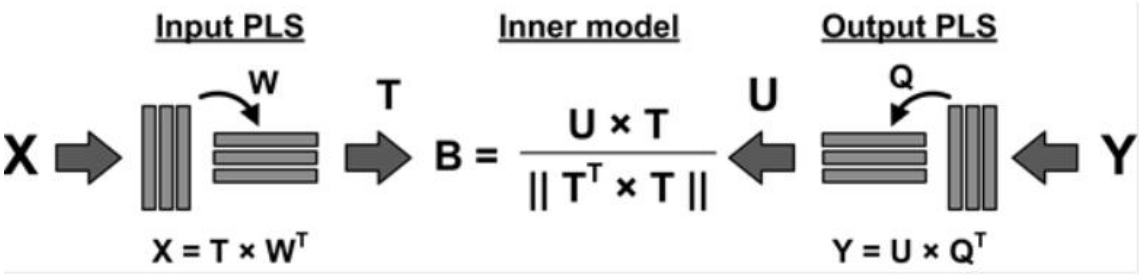

Figure 3. Schematic representation of PLS model. Left side represents the independent variables or inputs and the right side represents the dependent variables or outputs. Both sets of variables are decomposed into scores, T and U, and loadings, W and Q. The scores are then regressed against each other resulting in a diagonal matrix with the regression coefficients, B (adapted from Ferreira et al. [48]).

PLS: Pretreatment and Cross Validation

Before doing any type of regression analysis and because data sets differ in range and size, a pretreatment of the data was made. This is usually performed by scaling the data. That way each variable can have the same weight when there is an absence of knowledge about the relative importance of the variables. This scaling consists in center each variable by subtracting their averages and by dividing them by its standard deviation, the so called, auto-scaling [41, 49].

The accuracy of the predictions depend on the number of latent variables. This number tells us how good the model is in a way that it consistently precisely predicts the intracellular flux distribution, Y, with new medium concentrations, X. If one uses a low number of LV, information can be lost, but since data is never noise free, some variables will only add noise, so a high number of LV is also not desirable [50]. In order to create a valid PLS model with optimal prediction power, a cross validation technique was applied to determine the optimal number of latent variables [41, 42].

In this case, single cross validation technique was applied. With this technique, part of the data, in this case 1/3 of it, was removed from both independent set and dependent set and used as validation set. The remainder that forms the training set was used to develop several training models in which each model was based on one LV. In order to identify which LV gave a better prediction power, one to many LV were tested, so for instance the first training model was based on 1LV, the second was based in 2LV and so on and so forth. For each of the training model, a prediction of the validation set was made and the respecting modelling errors were calculated. These errors were calculated based on the difference between the actual values of the validation set (measured values) and the values predicted by the training model (observed values). The sum of squares of the errors was then calculated as the sum of squares of all squared errors. The model with the lowest error was selected as the best and, consequently the number of LV [50, 51].

PLS: PLS model

The PLS model was built using the complete data set for both Y and X and the number of LV estimated with the cross validation technique. With the algorithm npls (Copyright (C) 1995-2006 Rasmus Bro & Claus Andersson; Copenhagen University, DK-1958 Frederiksberg, Denmark, rb@life.ku.dk) the best model parameters values i.e., scores, loadings and the regression coefficient matrix were calculated. With such parameters and with the algorithm npred (Copyright (C) 1995-2006 Rasmus Bro & Claus Andersson; Copenhagen University, DK-1958 Frederiksberg, Denmark, rb@life.ku.dk), new input sets were used to make flux predictions.

With the PLS model established, it was finally possible to evaluate the impact of the medium concentration into each flux distribution and to elaborate strategies for the optimizations proposed.

PLS: Optimization for a continuous system

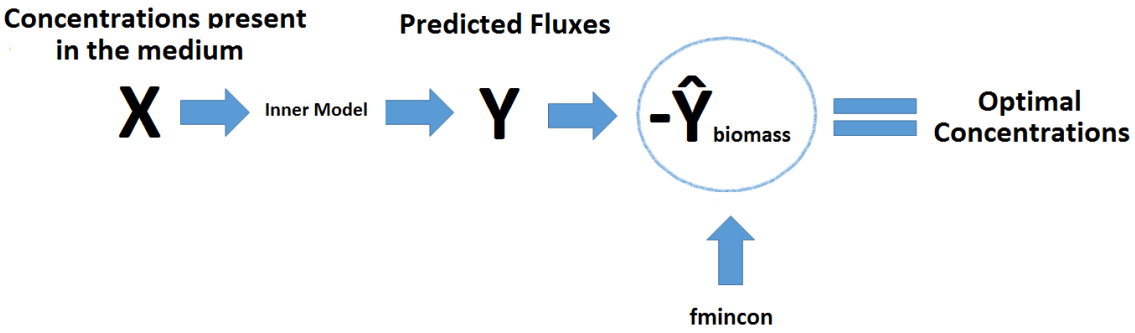

Figure 4. After the selection of the inputs through the PLS model, new predictions were made. Being the biomass growth rate, the rate of interest a mathematical maximization function, fmincon (MATLAB, the Mathworks, 2013) was applied in order to determine the optimal medium concentrations that resulted in a maximization of the biomass growth rate.

When performing a continuous operational mode, fresh medium is constantly added and spent medium is collected so the extracellular environment is inalterable over time [18]. This means that given a specific set of inputs or concentrations the intracellular rates will also be constant including the biomass growth rate. Therefore, optimal concentrations that would result in a maximum biomass growth rate would lead to high cell densities.

Using the PLS model, several sets of medium concentrations based on the experimental data were used as inputs and new predictions were made. The selection of the input was made by evaluating which one had the best prediction of the biomass growth rate.

Finally, a mathematical maximization function (fmincon; MATLAB, the Mathworks, 2013), was used to optimize the input set in a way that a highest biomass growth rate would be obtained (Figure 4).

PLS: Optimization for a Batch system

In this case, since the extracellular concentrations change over time the intracellular fluxes also change so a different approach had to be considered. In this case, the goal is to maximize the biomass concentration at the end of the batch, tf (Figure 5). Again the set of concentrations was selected based on the performance it had on the biomass growth rate. A time range and an additional value corresponding to the initial biomass had also to be considered. New fluxes were predicted by the PLS model and by multiplying their value with the initial biomass the derivatives of the concentrations were calculated. Next, with solver function (ode45; MATLAB, the Mathworks, 2013) integration of the derivatives was made in order to calculate the concentration values over time. Finally, the maximization function was used once again to determine the optimal concentrations that contributed to a maximum value of the biomass concentration.

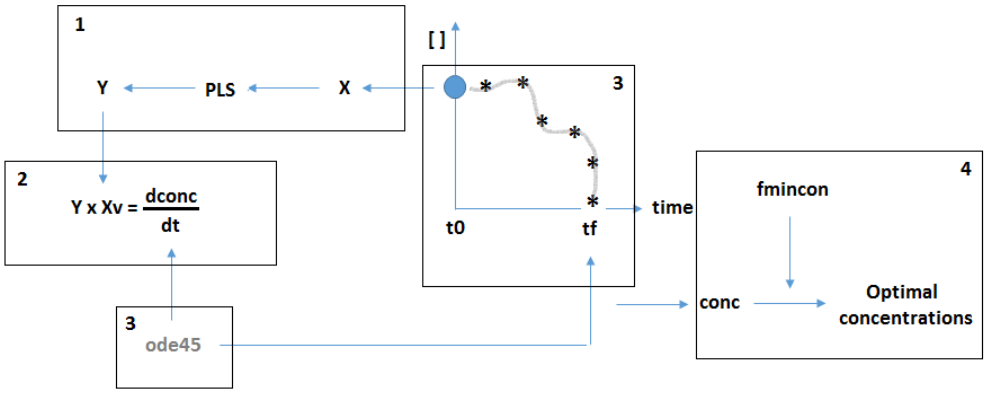

Figure 5. Given a specific set of concentrations, X, previously calculated by the PLS model a new PLS is applied and new fluxes are calculated, Y. (2) By multiplying the new fluxes with the biomass we obtain the derivatives of the concentrations. (3) Using solver function ode45, integrals are calculated from t0 to tf and as a result, concentration values are obtained for every time point. (4) Given the biomass concentration, fmincon is applied in order to determine the optimal concentrations that maximize the biomass growth.

Results and discussion

In this work, the impact of the medium concentrations on the flux distribution is studied and an optimization strategy is proposed in order to reach high cell densities for both a batch and a continuous system.

For that, calculation of the cell fluxome is made using classical metabolic flux analysis, which is then linked to the extracellular environment using a PLS model.

Since MFA is based on the quasi steady-state assumption, the intracellular metabolite concentrations should be constant over time (see Materials and Methods). That said, the time range considered was comprehended from moments after the exponential phase had begun until moments before the infection had been made. During this interval, it is expected that the quasi steady-state assumption holds (example in Figure 6).

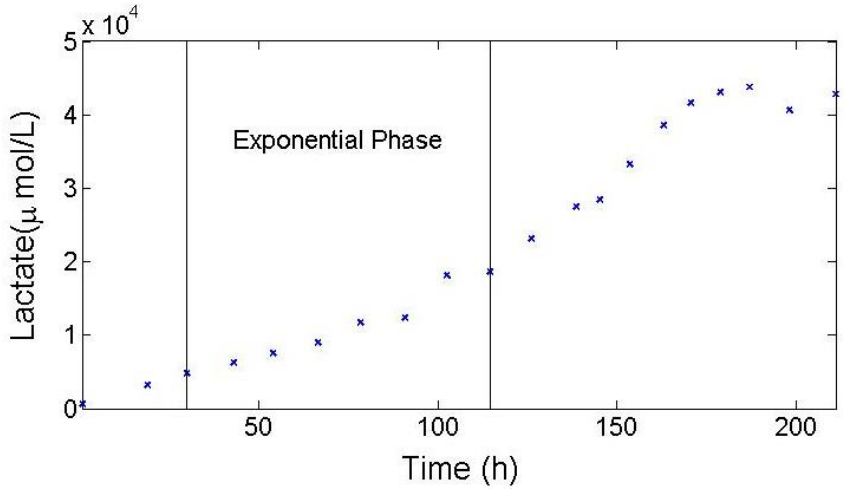

Figure 6. Concentration profile of Lactate excretion over time for Cultivation 1. Solid lines represent the time range defined.

Spline interpolation

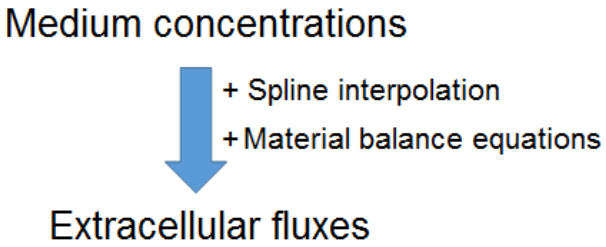

Figure 7. First steps applied in the medium concentrations in order to calculate the extracellular fluxes.

After defining the time range, a functional representation was made using cubic smoothing splines. With this interpolation, medium concentrations were calculated along

the time and by applying material balance equations the extracellular flux values were calculated (Figure 7).

Before estimating the intracellular fluxes with MFA, a detailed analysis of the cell metabolism was made based on the evaluation of each medium concentration, in order to see whether the cell was behaving as expected or not.

MDCK Metabolism

Because the same cell line and medium (SMIF8) were used in all cultivations, a similar behavior in terms of metabolism was expected. (Note that the cell line used in C3, MDCK.SUS2, derives from the cell line used in the other cultivations).

However, since the cultivations were not performed at the same time, and since the medium composition changes along the time, the initial concentrations were not the same resulting into a different metabolism by the cell in each cultivation, i.e. different flux distributions.

Moreover, C4 was operated in a distinct operational system, namely a wave reactor, which according to Lohr et al also influences the cell metabolism [15].

Carbon source metabolism

The primary carbon sources for ATP production are glucose and glutamine. They are also responsible for the production of waste products. According to the literature, the metabolism of these two components leads to the production of ammonia and lactate, components known to inhibit the cell growth. Ammonia results from the metabolism of amino acids, mainly from glutamine degradation, and lactate is synthesized from the conversion of glucose to pyruvate during the glycolytic pathway [52]. Figure 8 and figure 9 demonstrate the metabolism of these compounds.

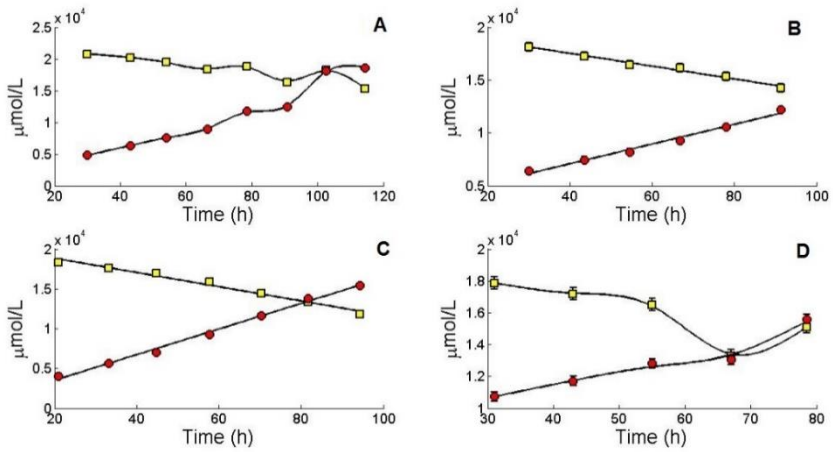

Figure 8. Concentration values for lactate release and glucose uptake during the exponential phase of MDCK suspension cells with respective standard deviations. (A) Represents the first cultivation; (B) represents the second cultivation; (C) represents the third cultivation; (D) represents the fourth cultivation; glc ( ), lac ( ).

Looking at the representations, it seems that most of the glucose up taken by the cell is transformed to lactate, as expected. Comparing all cultivations, C1, presents the highest lactate concentration compared to the other cultivations.

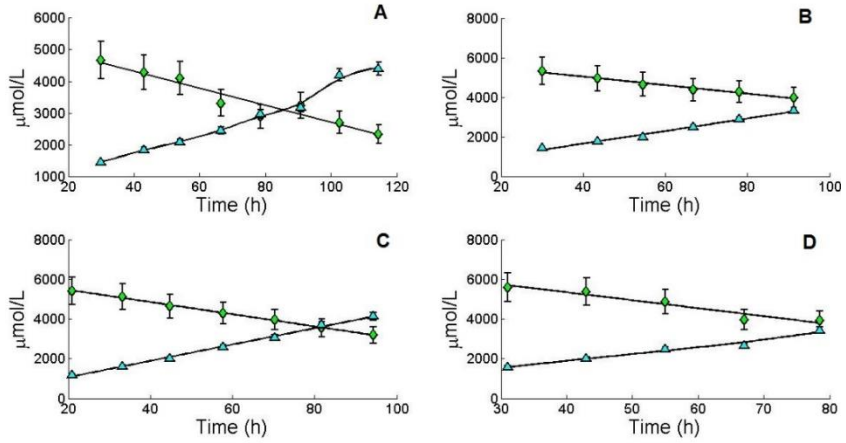

Figure 9. Concentration values for ammonia release and glutamine uptake during the exponential phase of MDCK suspension cells with respective standard deviations. (A) Represents the first cultivation; (B) represents the second cultivation; (C) represents the third cultivation; (D) represents the fourth cultivation; gln (◇), NH3 (△).

In the case of glutamine consumption and ammonia excretion, results also seem to be in accordance to what is expected, as most of the glutamine is converted to ammonia. Starting concentrations of glutamine are close to 6000 µmol which according to V. Lohr et. al. [15] the risk of reaching inhibiting ammonia concentrations is high. Again, C1 presents the highest ammonia concentration compared to the other cultivations. C1 had the higher initial concentration of glucose (20780.97 µmol/L) when compared to the other cultivations (18134.54 µmol/L for C2; 18315.47 µmol/L for C3; and 17868.49 µmol/L for C4) so a higher concentration of lactate was expected, however C4 had the higher initial concentration of glutamine (5600.94 µmol/L) when compared to the other cultivations (4672.29 µmol/L for C1; 5320.69 µmol/L for C2; and 5417.59 µmol/L for C3) so higher concentrations of ammonia were expected for this cultivation. It might be that, in C1 other pathways than the usual are contributing for the production of ammonia leading to such high values.

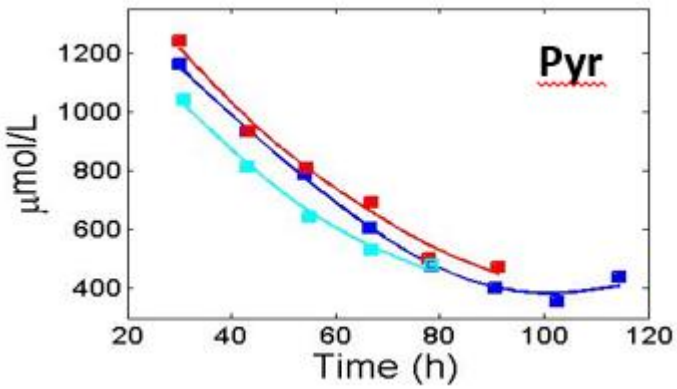

Figure 10. Concentration values for the uptake of pyruvate during the exponential phase of MDCK suspension cells. Dark blue represents the first cultivation; red represents the second cultivation; light blue represents the fourth cultivation.

Pyruvate is an intermediate of lactate production [11], so a decrease over time is expected as it is shown in Figure 10. Data not shown for C3 as not enough measurements were made.

Metabolism of essential and non-essential amino acids

Essential amino acids (e.g., histidine, isoleucine, leucine, methionine, phenylalanine, threonine, tryptophan and valine) were consumed by the cell in all cultivations, as expected. In contrast to the essential amino acids, part of the non-essential amino acids were consumed whilst others were released. Arginine, cysteine, tyrosine and aspartate concentrations showed a decrease over time, while alanine and glycine concentrations increased. Asparagine concentration was almost constant during the considered time. Glutamate concentration showed not only a decrease over time but also several oscillations, which might affect the calculation of both extracellular and intracellular fluxes. Due to problems in the experimental data from proline and serine measurements could not by analyzed. For a better understanding see Annex 1.

Biomass synthesis

Since our goal is to understand how the extracellular environment affects the cell regulation (i.e., flux distribution) in order to reach high cell densities, both viable biomass concentration and biomass growth rate were evaluated during the exponential phase to be compared with the future results (Figure 11).

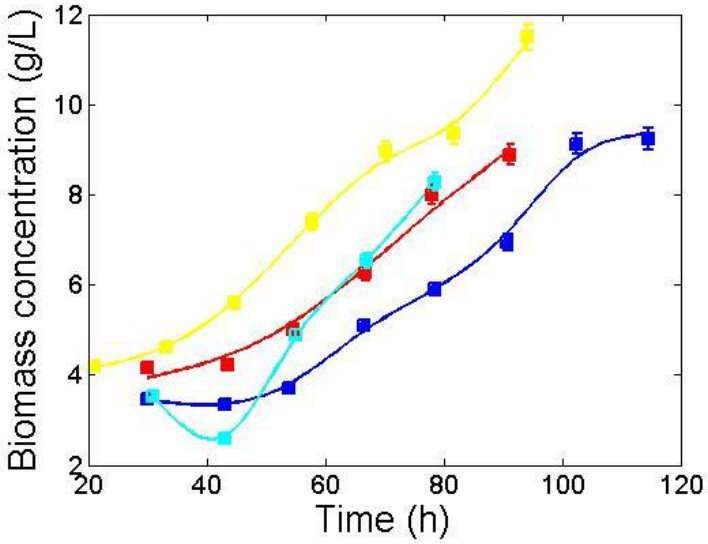

Figure 11. Biomass concentration during the exponential phase of MDCK suspension cells for all cultivations. The solid lines represent the model fit. Cultivation 1 is represented in dark blue and has a final cell density of 9.24 g/L; Cultivation 2 is represented in red and has a final cell density of 8.88 g/L; Cultivation 3 is represented in yellow and has a final cell density of 11.50 g/L; Cultivation 4 is represented by light blue and has a final cell density of 8.28 g/L.

Biomass growth rates were calculated with a linear regression model (data not shown). The first three cultivations resulted in similar growth rates ≈ 0.014 h^{-1}, which corresponds to a duplication time of 49 hours and 51 minutes. C4 presented the highest

biomass growth rate (0.022 h^{-1}) resulting in a duplication time of 31 hours and 51 minutes.

Table 3. Final cell density (g/L), biomass growth rate (h-1) and duplication time (h) for all cultivations during the exponential phase.

	C1	C2	C3	C4
Duration of the exponential phase (h)	84.5	61.25	73.24	47.5
Final cell density (g/L)	9.24	8.88	11.50	8.28
Biomass growth rate (h^{-1})	0.014	0.014	0.014	0.022
Duplication Time	49h 51 min	49h 51 min	49h 51 min	31h 51 min

Observing Table 3, a few considerations can be outlined. Since C1 has the longest exponential phase, higher biomass concentrations were expected. However, C3, which shows the second longest phase, presents higher values. As told before, more lactate and ammonia were produced in C1 so there might be occurring some inhibition affecting the cell growth, even though both cultivations show the same biomass growth rate [53, 54].

C4 has almost half of the duration of C1 and yet their final cell density is similar. This can be explained by the fact that C4 has a higher biomass growth rate and also because C4 is operated in a wave bioreactor. These types of operational systems have already proven to reach higher cell densities and lower duplication times when compared to stirred-tank bioreactors [15].

Metabolic Flux Analysis

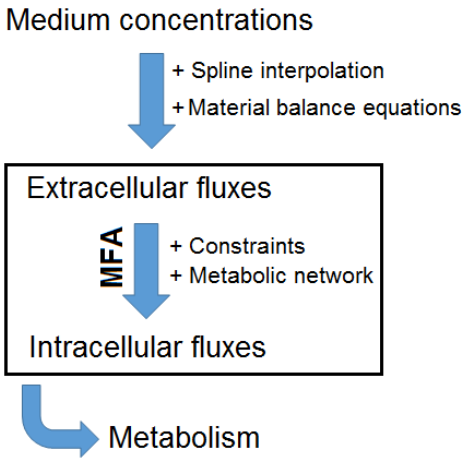

Figure 12. Overview of all the steps performed in the experimental data in order to evaluate the cell metabolism.

As mentioned before, MFA is a constraint based-model that permits the calculation of the flux distribution (see Materials and Methods). At this point, the extracellular fluxes were estimated from the medium concentrations using spline approximations and material balance equations. Also, a metabolic network had already been selected and the constraints defined (Figure 12).

Extracellular flux distribution

Firstly an analysis of the extracellular fluxes was made. A positive signal means that the reactions are carried in the direction of the arrow and the negative signal means that the reactions are carried out in the opposite direction of the arrow.

Highest flux values are registered for glucose and lactate. Since glucose is the main source of ATP and because the cell does not function without it, a high rate for the consumption of this compound is expected and since lactate is the resulting product from the consumption of glucose, a high lactate rate is also expectable.

Regarding the other elements, most of them seem to have similar rates. C4 presents high flux values for most of the compounds, meaning that in this case, the cell metabolism should be more active, which, as seen before, is expected since this cultivation is operated in a wave bioreactor.

The direction of the fluxes also seem to be in accordance with the literature, except for glutamate which appears to be in the opposite direction. As seen in the Materials and Methods section, one of the MFA constraints is the quasi steady-state assumption, which signifies that the metabolite concentrations should be constant over time. As mentioned before, glutamate shows several oscillations which might be affecting the calculation of the fluxes.

Table 4. Average extracellular fluxes (µmol/cell/h) and respective standard deviations calculated using a Monte Carlo approach during the time range considered for each cultivation.

	Reaction	C1	C2	C3	C4
Gln	0.33 ATP_c ==> GLN_c	3.04 ± 1.10	1.29 ± 2.06	2.49 ± 1.26	5.82 ± 3.68
NH_3	<==> NH3_c	-4.06 ± 1.69	-2.98 ± 0.45	-4.05 ± 0.36	-4.81 ± 1.14
Glc	Glc → Glc_c	12.20 ± 9.08	10.82 ± 1.40	13.54 ± 0.96	15.28 ± 10.77
Lac	<==> Lac_c	-29.61 ± 6.92	-16.63 ± 1.12	-24.38 ± 0.85	-21.53 ± 5.82
Glu	ATP_c ==> GLU_c	-1.33 ± 0.35	-0.54 ± 0.31	-0.32 ± 0.18	-2.07 ± 0.48
Pyr	0.33 ATP_c ==> Pyr_c	2.17 ± 0.07	2.41 ± 0.08	0.00 ± 0.00	3.14 ± 0.11
Arg	0.33 ATP_c ==> ARG_c	0.36 ± 0.34	0.61 ± 0.31	0.54 ± 0.18	0.80 ± 0.49
Asn	0.33 ATP_c ==> ASN_c	0.01 ± 0.25	0.46 ± 1.04	0.18 ± 0.63	0.71 ± 0.65
Ala	ALA_c ==>	2.37 ± 0.21	2.71 ± 1.12	5.66 ± 1.91	2.77 ± 0.48
Thr	0.33 ATP_c ==> THR_c	0.17 ± 0.16	0.44 ± 0.23	0.43 ± 0.13	0.55 ± 0.20

Gly	GLY_c ==>	0.36 ± 0.13	0.14 ± 0.44	0.34 ± 0.61	0.02 ± 0.24
Val	0.33 ATP_c ==> VAL_c	0.55 ± 0.07	0.37 ± 0.09	0.53 ± 0.21	0.96 ± 0.16
Ile	0.33 ATP_c ==> ILE_c	1.06 ± 0.22	1.16 ± 0.79	1.00 ± 0.19	2.00 ± 0.52
Leu	0.33 ATP_c ==> LEU_c	0.98 ± 0.22	1.30 ± 0.28	1.05 ± 0.31	2.29 ± 0.27
Met	0.33 ATP_c ==> MET_c	0.15 ± 0.09	0.15 ± 0.12	0.17 ± 0.08	0.42 ± 0.19
His	0.33 ATP_c ==> HIS_c	0.12 ± 0.10	0.10 ± 0.04	0.13 ± 0.03	0.26 ± 0.08
Phe	0.33 ATP_c ==> PHE_c	0.13 ± 0.07	0.22 ± 0.10	0.04 ± 0.38	0.40 ± 0.16
Asp	ATP_c ==> ASP_c	1.88 ± 0.00	2.69 ± 0.00	3.78 ± 0.00	4.07 ± 0.00
Cys	0.33 ATP_c ==> CYS_c	0.06 ± 1.62	0.08 ± 2.33	0.09 ± 1.69	0.21 ± 4.17
Tyr	0.33 ATP_c ==> TYR_c	0.10 ± 0.09	0.10 ± 0.02	0.14 ± 0.01	0.33 ± 0.11
Trp	0.33 ATP_c ==> TRP_c	0.04 ± 0.13	0.03 ± 0.03	0.05 ± 0.06	0.09 ± 0.05

Intracellular flux distribution

Secondly, the MFA model performed the estimation of the intracellular fluxes. Here, a detailed analysis was made (Table 5).

Table 5. Average intracellular fluxes estimated by MFA (µmol/cell/h) during the time range considered for each cultivation.

No.	Reaction	C1	C2	C3	C4
	Glycolysis				
66	Glc_c ==> G-6P_c	12.20	10.82	13.54	15.28
2	G-6P_c <==> F-6P_c	13.73	6.21	11.49	7.61
3	F-6P_c <==> GAP_c	12.27	4.23	9.59	5.00
55	GAP_c <==> PGA_c	22.61	5.87	16.68	6.57
56	PGA_c <==> PEP_c	22.61	5.87	16.68	6.57
57	PEP_c ==> Pyr_c	45.19	22.26	29.79	30.70
	Pentose Phosphate Pathway (PPP)				
60	R-5P_c <==> F-6P_c + GAP_c	-0.73	-0.99	-0.95	-1.31
61	R-5P_c <==> GAP_c + S-7P_c	-0.73	-0.99	-0.95	-1.31
62	GAP_c + S-7P_c <==> F-6P_c	-0.73	-0.99	-0.95	-1.31
	Anaplerotic Reactions				
5	Pyr_m ==> A-CoA_m	-1.18	-1.57	-1.52	-1.77
6	Mal_m <==> Pyr_m	-23.07	-13.39	-6.27	-21.54
68	Mal_c <==> Pyr_c	8.90	12.04	11.57	15.84
69	OAA_c <==> PEP_c	22.58	16.39	13.12	24.13

	TCA cycle				
7	A-CoA_m + OAA_m ==> Cit_m	7.56	8.92	8.40	11.12
71	Cit_m <==> a-Ket_m	0.54	-0.55	-0.73	-1.40
10	a-Ket_m ==> S-CoA_m	1.51	6.30	8.43	8.14
104	S-CoA_m <==> Fum_m	8.73	13.87	16.12	16.67
9	Fum_m <==> Mal_m	8.73	13.87	16.12	16.67
8	Mal_m <==> OAA_m	7.56	8.92	8.40	11.12
72	Mal_c <==> OAA_c	16.91	8.41	4.44	14.03
74	Cit_c ==> OAA_c + A-CoA_c	7.02	9.48	9.13	12.53
	Amino acid degradation				
11	GLU_m <==> a-Ket_m	7.16	12.44	13.18	13.66
12	GLN_c <==> GLU_c	1.24	-1.77	-0.18	0.47
16	ALA_c <==> Pyr_c	-3.45	-4.63	-7.46	-6.04
18	ASP_c <==> OAA_c	-1.35	-1.50	-0.46	-2.42
42	ARG_c <==> GLU_c	2.00	1.78	2.14	0.91
43	ASN_c <==> ASP_c	-0.43	-0.25	-0.54	-1.05
45	ILE_c ==> S-CoA_m + A-CoA_m	2.99	3.56	3.33	4.54
46	LEU_c ==> A-CoA_m	1.38	1.58	1.51	1.86
48	MET_c ==> S-CoA_m	1.02	0.63	1.01	0.12
50	PRO_c <==> GLU_c	-7.32	-1.33	-1.10	-1.56
51	THR_c ==> Pyr_c	1.03	0.92	1.11	0.11
52	TRP_c ==> A-CoA_m	0.80	1.10	1.04	1.39
53	VAL_c ==> S-CoA_m	3.21	3.38	3.34	3.88
77	GLY_m <==> SER_m	-3.00	-4.12	-4.05	-6.02
78	SER_c <==> Pyr_c	-3.74	-5.96	-7.51	-3.85
80	CYS_c ==> Pyr_c	1.41	1.42	1.63	1.42
	Other reactions				
13	Pyr_c <==> Lac_c	29.61	16.63	24.38	21.53
79	NADH_m <==> NADPH_m	15.92	0.96	-6.90	7.88
	Lipid Biosynthesis				
87	CH	0.18	0.24	0.23	0.32
88	PC	0.68	0.92	0.88	1.21
89	PE	0.26	0.35	0.33	0.46
90	PS	0.03	0.03	0.03	0.05
91	PG	0.07	0.09	0.09	0.12
92	PI	0.09	0.13	0.12	0.17
93	SM	0.08	0.11	0.11	0.15
	Respiration reactions				
75	FADH2_m ==> ATP_m	18.22	24.51	26.54	28.58
24	NADH_m ==> ATP_m	2.10	21.44	31.02	16.62

	Membrane Transport (c – m)				
58	Pyr_c <==> Pyr_m	20.87	10.91	3.64	19.67
73	Mal_c + Cit_m <==> Mal_m + Cit_c	7.02	9.48	9.13	12.53
59	a-Ket_m <==> a-ket_c	6.18	5.59	4.02	4.12
86	Mal_m <==> Mal_c	31.27	27.82	23.12	39.62
76	ATP_m <==> ATP_c	35.92	98.48	127.62	94.57
82	GLU_c <==> GLU_m	7.16	12.44	13.18	13.66
103	SER_c <==> SER_m	3.00	4.12	4.05	6.02
102	GLY_c <==> GLY_m	-6.00	-8.23	-8.10	-12.05
84	NH3_c <==> NH3_m	-4.16	-8.32	-9.13	-7.64
70	CO2_c <==> CO2_m	22.58	10.24	0.97	19.73
	Membrane transport (m – c)				
22	<==> CO2_c	-11.87	-20.53	-26.42	-21.90
25	==> O2_c	15.58	29.86	35.60	31.04
64	ATP_c ==>	13.26	9.57	63.87	-77.66
81	Urea_c <==>	2.00	1.78	2.14	0.91

Observing the flux values related to glycolysis, it seems that glucose is effectively converted to pyruvate (reaction 57). Pyruvate can then be carried from the cytoplasm to the mitochondria and undergo to anaplerotic reactions or it can be converted to lactate**.** Although there is some pyruvate being transported to the mitochondria (reaction 58), most of it is converted to lactate as indicated by the highest fluxes (reaction 13). Concerning PPP, flux values were low and stayed constant along the reactions (reactions 60 to 62).

The anaplerotic reactions are partly active. More activity is observed for the cytosolic reactions (reaction 68 and 69). As seen before, part of the pyruvate formed in the cytoplasm is transported to the mitochondria (reaction 58) and then converted to malate (reaction 6). Malate is transported to the cytoplasm (reaction 86) and metabolized again to pyruvate (reaction (68) and to oxaloacetate (reaction 72). Curiously the reaction carried out by pyruvate dehydrogenase operates in the opposite direction (reaction 5), demonstrating some inconsistency thought the magnitude of these flux values is relatively low in relation to other pyruvate fluxes. Since this occurs, no acetyl-CoA is produced.

Despite acetyl-CoA is not being produced during anaplerotic reactions, some activity is detected in the TCA cycle. In this case, the main precursors of this compound are isoleucine, leucine and tryptophan (reaction 45, 46 and 52).

Concerning the amino acid degradation and lipid biosynthesis, similar fluxes are observed for every cultivation, except for the reaction responsible for the production of glutamate from glutamine (reaction 12). In this case, only in C1 and C4 glutamine is converted to glutamate and C1 presents the highest conversion rate, meaning that this might be the pathway contributing for the high levels of ammonia as the latter compound is released in this reaction.

Between the two respiration reactions, both pathways showed more or less the same activity (reaction 24 and reaction 25).

The highest flux values are observed for ATP reactions (reaction 64 and 76).

Looking carefully, arginine degradation (reaction 42) seems to be responsible for the synthesis of urea (reaction 81).

Overall the cell is behaving as expected in all cultivations and not much discrepancies are observed when comparing the fluxes. Even though the consumption of glucose is similar for all cultivations, a much higher excretion of lactate is observed for C1 due to high conversion rates of pyruvate. In this case, there might be some other pathways contributing for the high conversion rate and because of that, more waste product is excreted affecting the biomass growth. As expected, due to a high extracellular activity, cultivation 4 shows, in most of the cases, a high intracellular activity when comparing with the other cultivations.

Consistency Index

In order to validate the MFA model, a consistency test was made, i.e. the consistency index (h value) was calculated along the cultivations, (Figure 13). It can be seen that all cultivations present an *h* value lower than the corresponding χ^2 value, meaning that the assumed biochemistry behind the metabolic network is consistent with the measured extracellular fluxes, validating the model (see Materials and Methods).

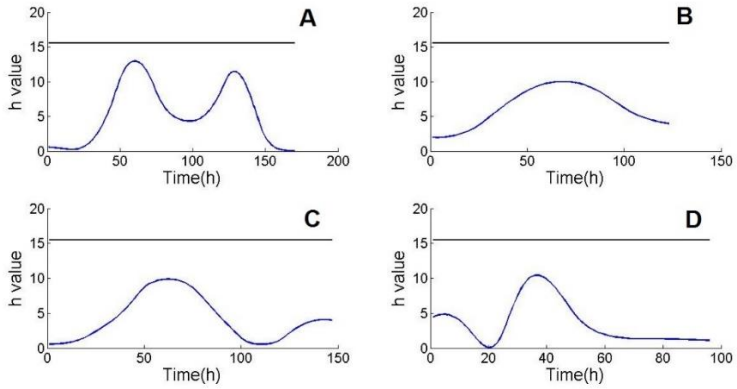

Figure 13. Consistency index (h) over time for each cultivation with test function (χ2 (0.95, 8) = 15.50). (A) Cultivation 1; (B) Cultivation 2; (C) Cultivation 3; (D) Cultivation 4.

Overview of the flux distribution

To get an impression of the flux distribution for each cultivation, a 3-D analysis was made (Figure 14).

As mentioned before all cultivations have different initial sets of concentrations leading, of course, to distinct flux distributions. The oscillations observed in each cultivation are the result of a different metabolism. Nevertheless, two reactions that present significant oscillations in every cultivation are the ones involving ATP, namely futile cycle reactions (represented by reaction 64) and ATP transport (reaction 76). As our model only considers basic metabolic pathways not all ATP-consuming reactions can be taken into account leading to errors in this case expressed through oscillations.

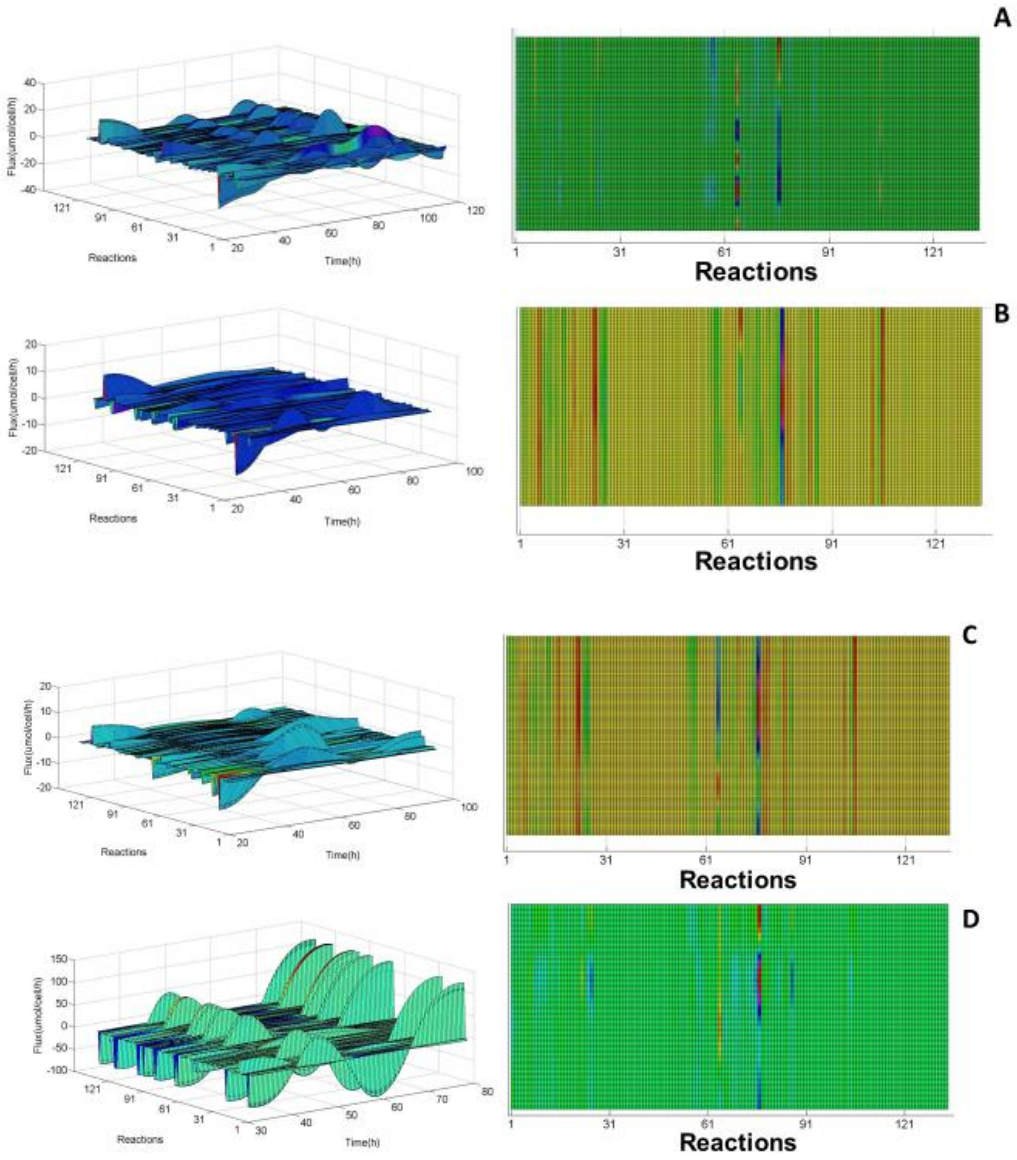

Figure 14. Metabolic flux distribution for all cultivations. (A) Cultivation 1; (B) Cultivation 2; (C) Cultivation 3; (D) Cultivation 4.

Partial Least Squares

Depending on the environment the cell will behave in a specific way, with a characteristic phenotypic trait, expressed as a result of the intracellular flux distribution.

Here the proposed method combines MFA with PLS to create a regression model between the input medium concentrations, estimated with material balance equations, and the output flux distribution, estimated through MFA. The result is then a matrix of regression coefficients representing how strongly each compound present in the medium correlates with each flux. This model can then be used to study the perturbation of the medium concentrations towards an increase in the biomass growth rate for a batch and a continuous system.

Number of latent variables

The first step in order to create a PLS model, was to determine the number of latent variables that would best decompose both sets of variables and, consequently result in a model with best predictive power. This was possible using cross validation techniques.

Cross validation is often used to validate a model. There are several cross validation techniques that can be used to serve this purpose. In this case, single cross validation technique was applied as seen in the Materials and Methods section.

The principal behind this technique is that the optimal number of LV corresponds to the minimum modelling error obtained for the estimation of the validation set.

Figure 15 shows the plot of the modelling error against the number of LV for the validation set when applying this technique. In this case, the minimum error found for the validation set corresponds to a number of LV equal to 11.

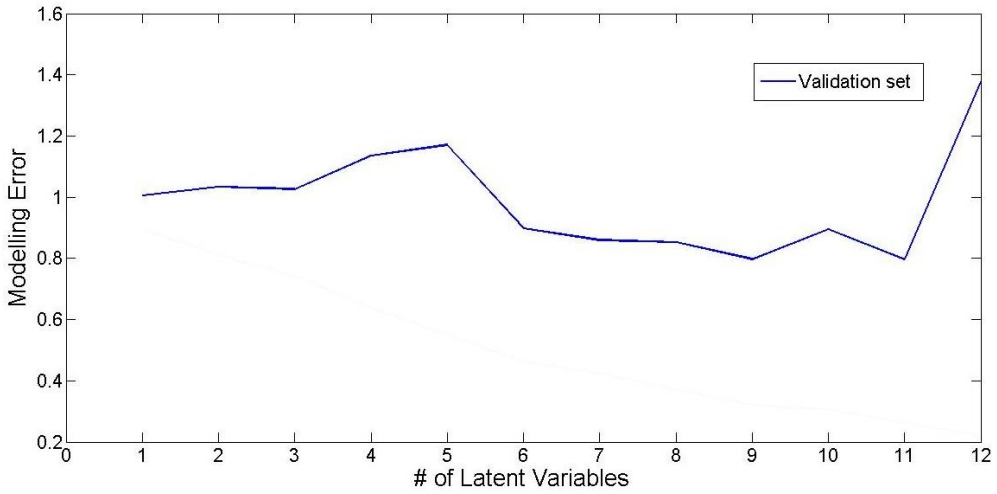

Figure 15. Modelling error obtained for each LV with single cross validation technique for the validation set.

What was seen is that as the number of LV increases, the error of the validation set also increases (data not shown). This means that with a high number of LV the predictions would only get worse as probably only noise or irrelevant data was being included in the model, affecting the predictions. Herein, the goal was to obtain a model based on the number of LV that could include all relevant data and at the same time minimize redundant data.

With 11 LV as it is represented in Table 6, the training model was able to explain almost 100% of the data from the extracellular concentrations and around 74% of the fluxome data.

Table 6. Training model decomposition results in terms of % of explained variance over number of latent variables.

Latent Variables	Variance X (%)	Variance Y (%)
1	57.98	10.22
2	79.34	18.54
3	86.54	25.62
4	90.47	35.90
5	93.75	45.03
6	95.35	53.76
7	98.47	57.28
8	99.01	62.78
9	99.18	67.78
10	99.49	69.41
11	99.61	73.68

PLS model

Having identified the number of LV, the PLS model was built. In this case the resulted model explained almost 70% of the variance in Y (Table 7).

Table 7. PLS model decomposition results in terms of % of explained variance over number of latent variables.

Latent Variables	Variance X (%)	Variance Y (%)
1	49.31	6.60
2	74.07	12.42
3	83.72	21.41
4	87.58	34.07
5	92.03	43.85
6	95.21	47.91
7	97.69	51.86
8	98.27	58.01
9	98.69	60.93
10	99.17	65.20
11	99.39	67.77

To have an indicator of the accuracy of the predictions, the predicted extracellular fluxes were plotted against the measured extracellular fluxes, Figure 16. The regression model clearly performed well for most of the fluxes, but not for all of them, e.g. ammonia, glucose, lactate and glutamate. The less good prediction are most probably due to variations in the measured concentration values that in turn cause variation in the flux values estimated using the smoothing spline. This explanation would also be supported

by the observation that the greatest deviations seem to have a cyclic behavior, which is an artifact coming from greater or lower measured concentration value.

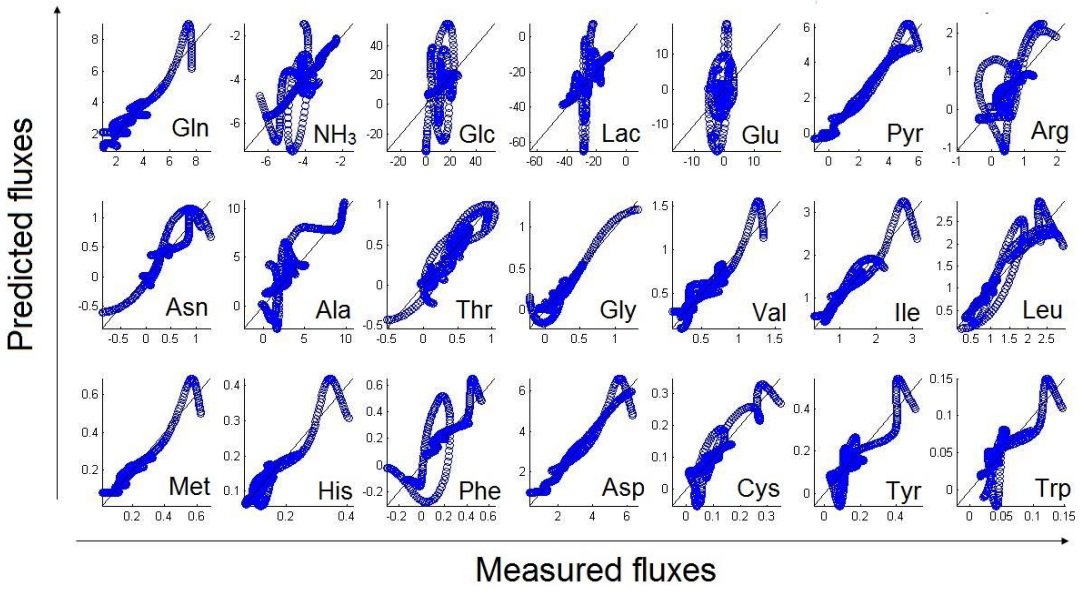

Figure 16. Correlation between predicted fluxes and measured fluxes.

Also very important is to analyze the model's specific biomass growth predictions. Although the model is capable to describe the general trend of biomass growth fairly well (Figure 17), it is not very precisely describing biomass growth. One cannot forget that our model can only explain almost 70% of the Y data.

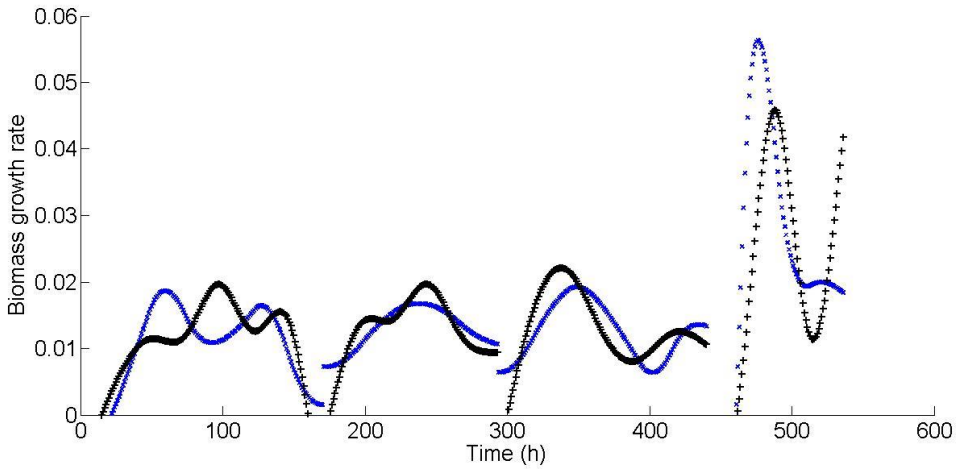

Figure 17. Prediction of the specific biomass growth rate (μ). Solid blue line represents the measured flux and solid black line represents the predicted flux.

The metabolic state of each cell, as the name implies has to do with the type of metabolism which the cell performs face to the conditions it finds. These conditions can range from the composition of the medium, the concentration of each component present in the medium to the cell's own needs.

A different medium will lead to a different metabolic state and consequently a different intracellular flux distribution. These differences may be visualized by one of the features of PLS, the 2-dimensional and the 3-dimensional score plotting.

It is clear that when a 3-dimensional plot is made, additional information is considered and different results are obtained when compared to a 2-dimensional plot. In both cases, the cultivation that stands out is cultivation 3 (Figure 18). In the 2-dimensional plot, while C1, C2 and C4 are close together, C3 stays more distant. On the other hand, on the 3-dimensional plot while C1, C2 and C4 present some oscillations, C3 has a more linear behavior. This means that C3 is in a different metabolic state which might be an influence of the medium composition since this cultivation has the same operating system as C1 and C2. The only thing different is the cell line that it is used, which as said before, should lead to no differences in terms of metabolism, since it derives from the cell line used in C1 and C2. Yet, as no pyruvate was considered for this cultivation (due to absence of measurements) it might be possible that the PLS model considers this cultivation to be in a distinct metabolic state. Not only pyruvate is known to be the intermediate of lactate production but it also has a huge role in the anaplerotic reactions which then affect all the other metabolic pathways such as the TCA cycle. Also, a much higher flux of the production of alanine was observed for this cultivation (Table 4).

This indicates that the PLS model can clearly identify that differences in the medium culture affect the intracellular flux distribution, in this case translated by differences in metabolic states.

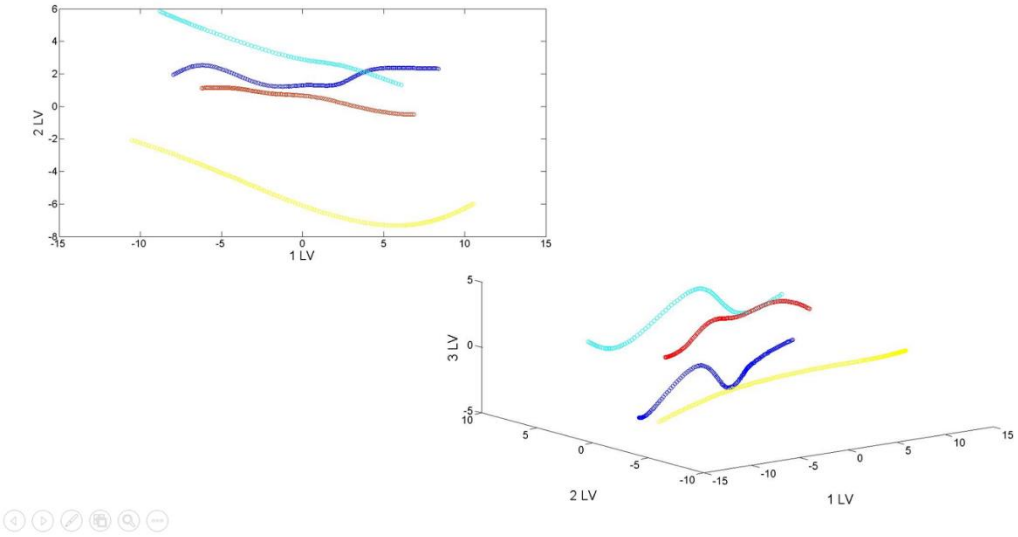

Figure 18. 2D score plot and 3D score plot from the PLS model. Cultivation 1 is represented in dark blue; Cultivation 2 is represented in red; Cultivation 3 is represented in yellow and; Cultivation 4 is represented in light blue.

To evaluate the impact of each component on each flux distribution, more precisely on the biomass growth rate, elasticities were evaluated in a form of a matrix map for each cultivation in the beginning and in the final time points considered (Figure 19 and Figure 20). The elasticities present sensitivities of the fluxes with respect to each component present in the extracellular medium and therefore with their concentrations. They are obtained by multiplying both loading sets (dependent and independent) with the regression coefficient matrix of the PLS model.

The dependencies collected in this matrix allow a qualitative prediction about the effects of perturbation on the flux distribution. In this case redness indicates a high correlation between a flux and a specific compound whereas blueness indicates a low

correlation. The compounds represented in light green seem to have less impact on the fluxes.

This color differentiation indicates that the PLS model was able to distinguish between informative variables and irrelevant data.

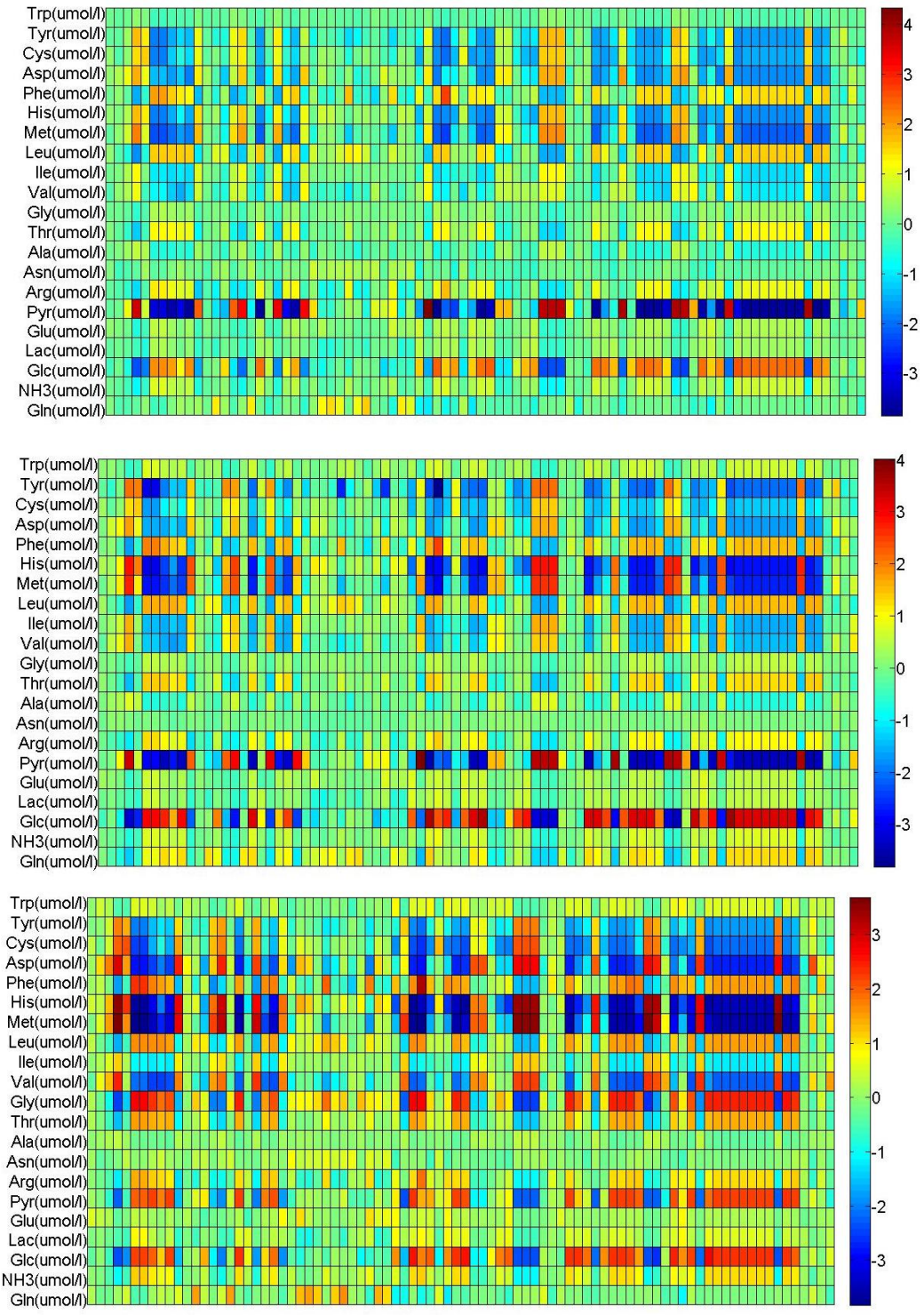

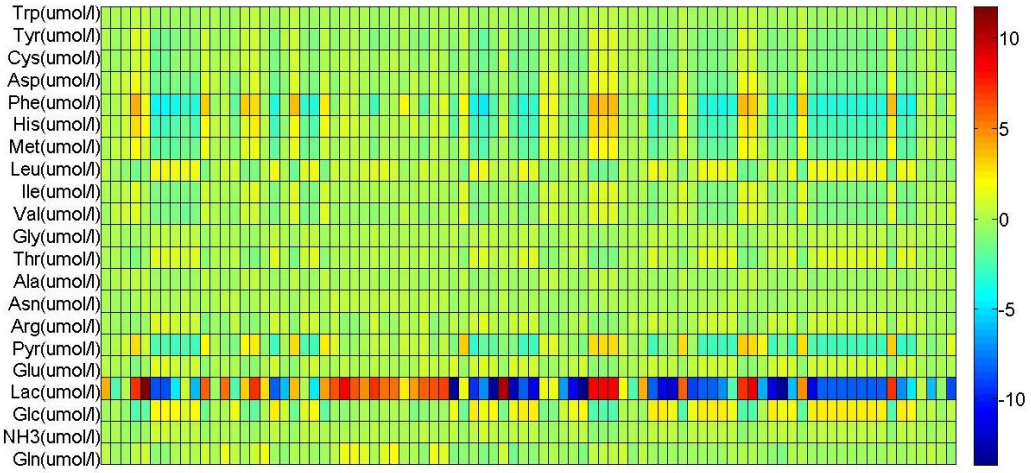

Figure 19. Elasticities of each intracellular flux with respect to each compound present in the medium for the initial time point for all cultivations (order of representation C1, C2, C3 and C4).

Observing Figure 19 what stands out are the different profiles that each cultivation presents slightly before the beginning of the exponential phase. This indicates that even though there were small differences in the initial set of concentrations for each cultivation the metabolism is strongly affected.

C1 and C2 are the cultivations with more resemblances. In these, glucose is the compound that correlates the most with the flux distribution than the remaining compounds. Being almost in the beginning of the exponential phase and being this compound one of the primary carbon sources such results were expected. Threonine, leucine and phenylalanine are also compounds which have a positive impact on the flux distribution though the correlation is not that accentuated. Pyruvate seems to have the lowest impact as well as valine, isoleucine, methionine, histidine, aspartate, cysteine and tyrosine. As for the remaining compounds they do not seem to have any impact at this time point.

As for C3 the same impact is verified as the previous cultivations except for pyruvate which in this case also has a high impact on the flux distribution. As seen before (Figure 10) no measurements were made for pyruvate in this cultivation, thus this absence might be influencing the PLS model to give such results, as it also had when evaluating the metabolic states of the cell.

C4 shows the most different profile being lactate the most active compound on the flux distribution. It might be that for the initial time point considered for this cultivation the cell was still in the lag phase and such still adapting to the environment. Additionally, the sensitivity values are much higher when compared to the other cultivations. Again the fact that this cultivation was operated in a wave bioreactor might be affecting in a more significant way the cell's metabolism.

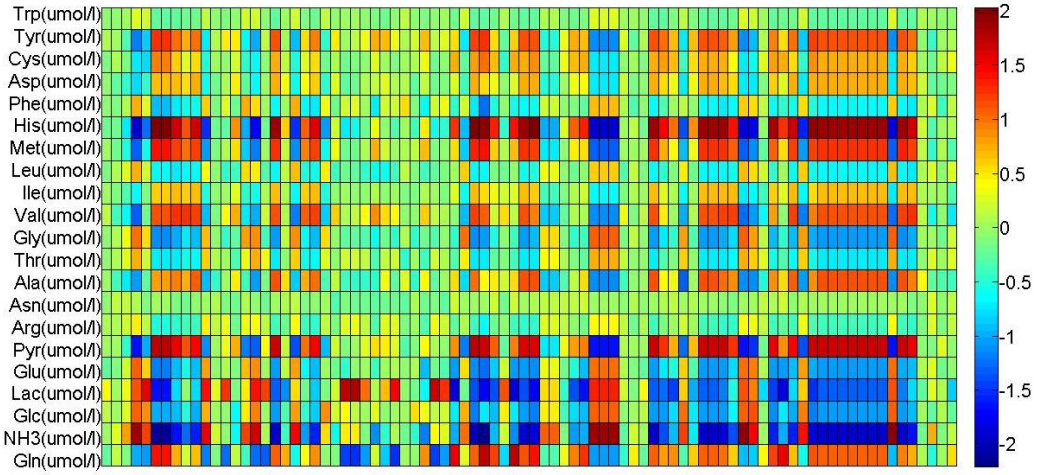
Trp(umol/l)
Tyr(umol/l)
Cys(umol/l)
Asp(umol/l)
Phe(umol/l)
His(umol/l)
Met(umol/l)
Leu(umol/l)
Ile(umol/l)
Val(umol/l)
Gly(umol/l)
Thr(umol/l)
Ala(umol/l)
Asn(umol/l)
Arg(umol/l)
Pyr(umol/l)
Glu(umol/l)
Lac(umol/l)
Glc(umol/l)
NH3(umol/l)
Gln(umol/l)
2
1.5
1
0.5
0
-0.5
-1
-1.5
-2

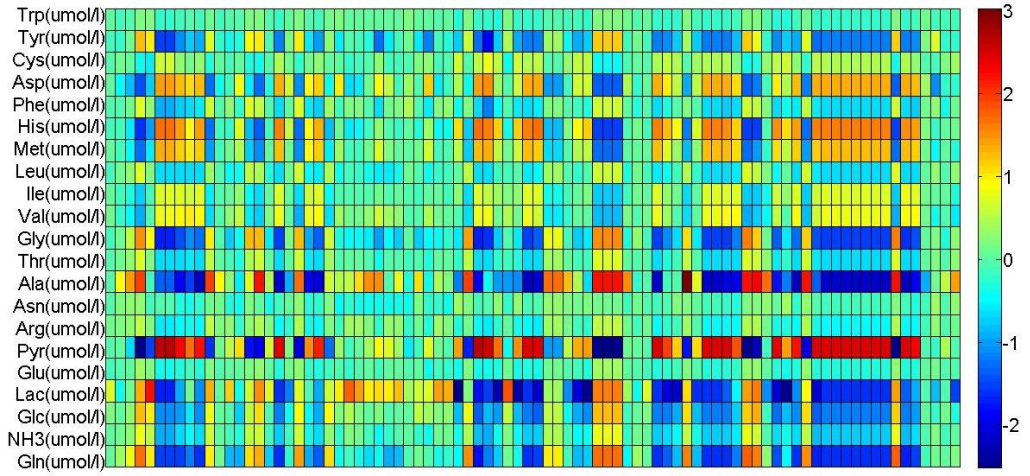
Trp(umol/l)
Tyr(umol/l)
Cys(umol/l)
Asp(umol/l)
Phe(umol/l)
His(umol/l)
Met(umol/l)
Leu(umol/l)
Ile(umol/l)
Val(umol/l)
Gly(umol/l)
Thr(umol/l)
Ala(umol/l)
Asn(umol/l)
Arg(umol/l)
Pyr(umol/l)
Glu(umol/l)
Lac(umol/l)
Glc(umol/l)
NH3(umol/l)
Gln(umol/l)
3
2
1
0
-1
-2

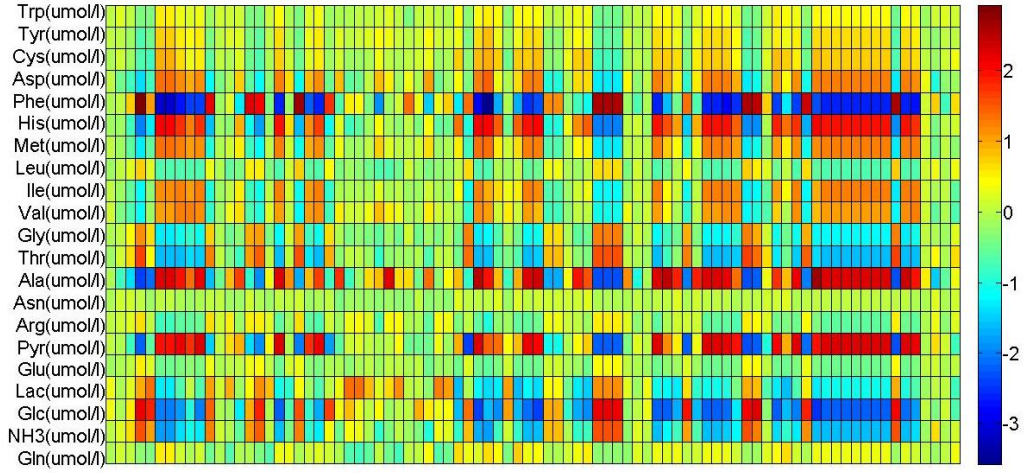
Trp(umol/l)
Tyr(umol/l)
Cys(umol/l)
Asp(umol/l)
Phe(umol/l)
His(umol/l)
Met(umol/l)
Leu(umol/l)
Ile(umol/l)
Val(umol/l)
Gly(umol/l)
Thr(umol/l)
Ala(umol/l)
Asn(umol/l)
Arg(umol/l)
Pyr(umol/l)
Glu(umol/l)
Lac(umol/l)
Glc(umol/l)
NH3(umol/l)
Gln(umol/l)
2
1
0
-1
-2
-3

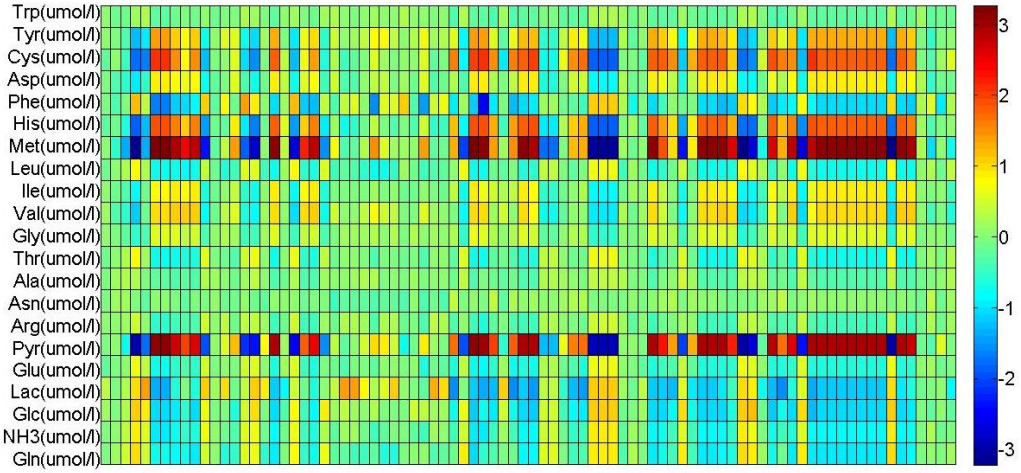

Figure 20. Elasticities of each intracellular flux with respect to each compound present in the medium for the final time point for all cultivations (order of representation C1, C2, C3 and C4).

Figure 20 shows the impact of the compounds on the flux distribution almost by the end of the exponential phase. Again, different profiles can be observed. At this stage the cell has already used all the nutrients and also excreted products and waste products so a different impact of the compounds is expected.

By this time high levels of lactate and ammonia are present in the extracellular medium of the cell. They are known to be toxic for the cell, thus a relative low impact on the flux distribution is seen for these compounds. In all cultivations pyruvate seems to have a significant impact on the flux distribution. Since at this time point the cell is reaching the end of the exponential phase, it means that there are large amounts of cells in the culture. Being glucose one of the primary carbon sources it is expected that most of it has already been consumed leaving pyruvate enough substrates to be converted to lactate. Histidine and methionine are other compounds which seem to have a positive impact in all cultivations and phenylalanine, leucine and threonine have a negative impact. So it seems that most of the compounds which before showed a low impact on the flux distribution now seem to have a higher impact, vice-versa.

Obviously that as time goes by, the environmental concentration changes according to the cell needs wherefore these impact changes demonstrate how the cell corresponds to the modifications in the environment by up and down-regulating certain pathways. A simple example is the consumption of glucose over time and the consequently pyruvate production and its impact on the cell. In the beginning (Figure 19), due to high concentrations, glucose had a high impact on the flux distribution and pyruvate had none, however as time went by its concentration decreased so as its impact whilst pyruvate concentration increased so as its impact (Figure 20).

The fact that the PLS model is able to keep track of the cell regulation towards the changes in the environment makes it suitable for being used in future optimizations.

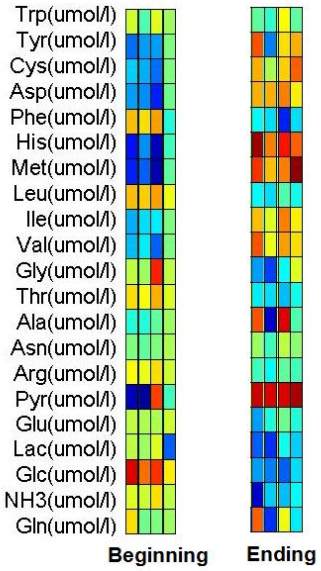

Figure 21. Elasticity for the biomass growth rate with respect to each component at the initial time point (left) and the final time point (right).

Figure 21 presents the sensitivities for the biomass growth rate at the initial and final time points considered. The results do not differ that much from the ones mentioned before. It seems that in the beginning, and with the concentrations that the cell encounters for each compound, that the biomass growth rate is strongly affected by glucose and part of it by phenylalanine, leucine and threonine. Then as time passes and their concentrations decrease, other elements begin to have a bigger importance such as tyrosine, cysteine, aspartate, histidine, methionine, isoleucine and valine and also pyruvate. The only compounds which seem to maintain their impact are asparagine and tryptophan. This means that once the initial compounds start to be limited, other compounds become more important, even though their concentration might also be decreasing. Note that the redness in pyruvate for C3 at the beginning has to do with the fact that no measurements were made influencing the results.

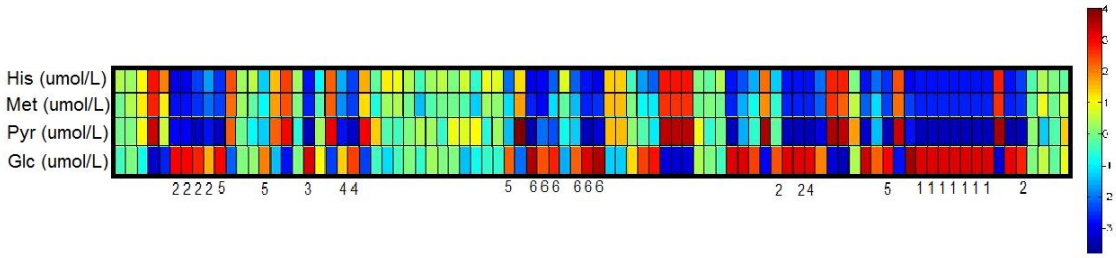

Figure 22. Pathway regulation by glucose, pyruvate, methionine and histidine for C1.

Another interesting aspect noticed with these results is the fact that in all cases demonstrated above, it seems that there is a certain group of reactions that are always regulated together, meaning that the same compound has the same effect in all of these pathways. This regulation is clearly exemplified in Figure 22. In the beginning and seen before, glucose is the compound that has the highest impact then the rest of the compounds and pyruvate, methionine and histidine are compounds with the lowest impact on the flux distribution. Looking carefully, the pathways that seem to be more affected (positively and negatively) are always the same. After an analysis some reactional groups were identified, being them 1) lipid biosynthesis; 2) TCA cycle; 3)

biomass growth rate; 4) respiration reactions; 5) glutamate involving reactions and; 6) essential amino acid degradation. For instance, if by knowing how to positively manipulate the lipid biosynthesis it might be that the same effect is verified for the remaining reactions present in the group, including the biomass growth rate, therefore new approaches can be tested.

The loading plot (Figure 23), another result obtained from the PLS model, shows the distribution of the medium components and the fluxes considered in a 3-dimensional way.

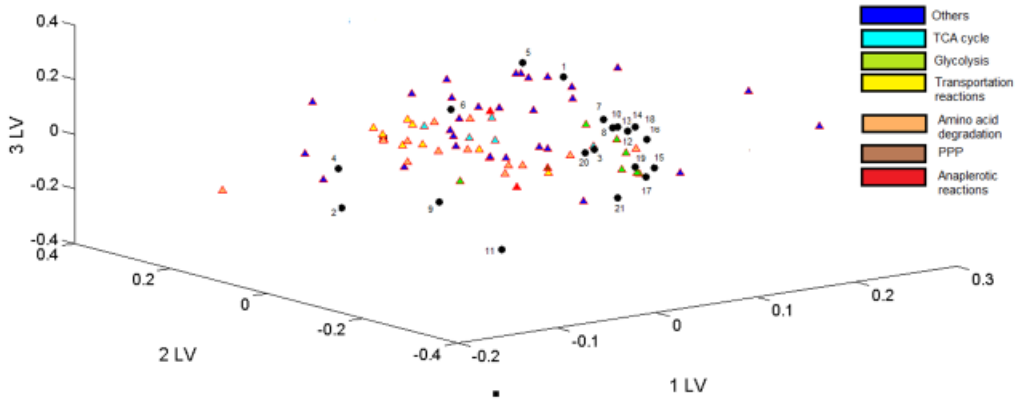

Figure 23 X loadings and Y loadings for 3 latent variables. (1) Gln, (2) NH3, (3) Glc, (4) Lac, (5) Glu, (6) Pyr, (7) Arg, (8) Asn, (9) Ala, (10) Thr, (11) Gly, (12) Val, (13) Ile, (14) Leu, (15) Met, (16) His, (17) Phe, (18) Asp, (19) Cys, (20) Tyr, 21 (Trp).

There is one distinct group in which the majority of the compounds are and there are few components which are isolated. On one hand we have ammonia (2) and lactate (4) both isolated and on the left part which are both known to be waste products. As identified on the image they are both close to their correspondent reactions. Then alanine (9) and glycine (11) are also isolated and in the center. Apart from the waste products mentioned before, these three components were the only ones being excreted by the cell. Pyruvate (6) seems to be close to the reactions concerning the TCA cycle and the anaplerotic reactions, which makes sense since this compound is involved in these pathways. The remaining compounds are close together and seem to form a cluster near the glycolytic reactions which also makes sense since glycolysis is the triggering pathway for all the other reactions. Strangely glutamine (1) and glutamate (5) are also isolated but they are known for having an important role on the cell growth [55]. Again, this might be a consequence of the measurements of the experimental data.

Continuous and batch optimization

For the optimizations proposed the strategies explained in the Materials and Methods section were applied and the selection of the input for the PLS model was based on the experimental data.

Both optimizations resulted in higher biomass growth rates reducing in more or less 10h the duplication time (Table 8).

Table 8. Comparison of the biomass growth rates (h^{-1}) and duplication time (h) obtained experimentally and with the batch and continuous optimizations.

	Biomass growth rate (h^{-1})	Duplication Time
Experimental	0.022	31h51min
Continuous optimization	0.034	20h21min
Batch optimization	0.030	22h73 min

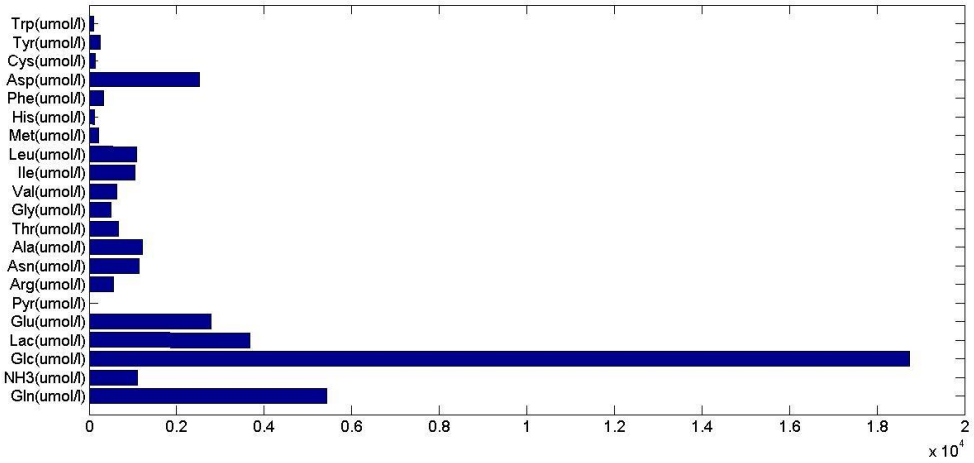

Figure 24. Optimal concentration for the continuous optimization.

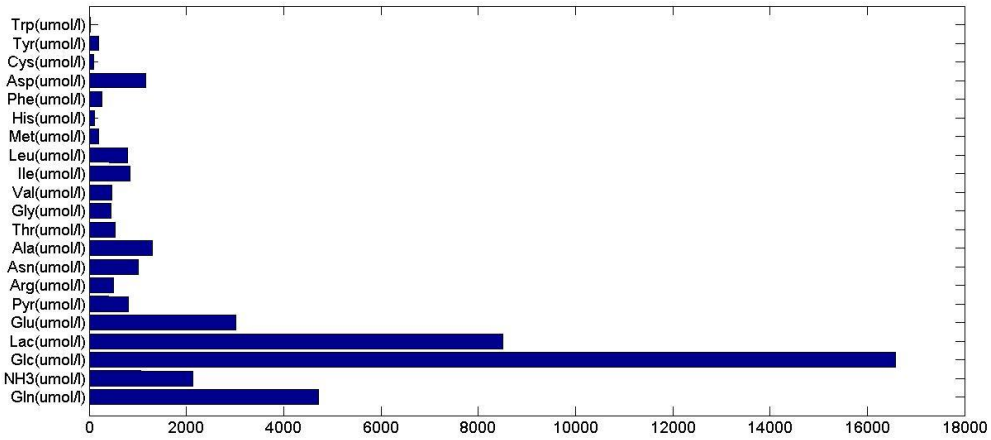

Figure 25. Initial optimal concentration for the batch optimization.

For each optimization, different information is collected. In the case of the continuous system (Figure 24), optimal concentration values were obtained. As they do not change over time, only a control of the dilution rate would be needed as hopefully a biomass growth rate of 0.034 h^{-1} would be achieved leading not only to a fast process but also to high densities than the ones obtained before.

In the case of the batch optimization (Figure 25) the concentrations at the beginning of the batch phase are manipulated by optimization. The medium

concentrations subsequently change over time. Controlling the initial concentrations is fairly easy and the encountered optimal concentrations could lead to a faster process with higher cell densities.

It can be seen that glucose is the component that presents the highest concentration in both optimizations as could be expected. Other components which also present high concentrations are glutamine, glutamate and aspartate. The fact that high concentrations of glutamate were obtained seems to reinforce the fact that the oscillations on the experimental data misguided the results concerning this compound.

An interesting aspect from the continuous optimization is the fact that almost no pyruvate is needed and still high biomass growth rates are achieved, thereby suggesting that this compound might not be necessary in the medium for this type of fermentation.

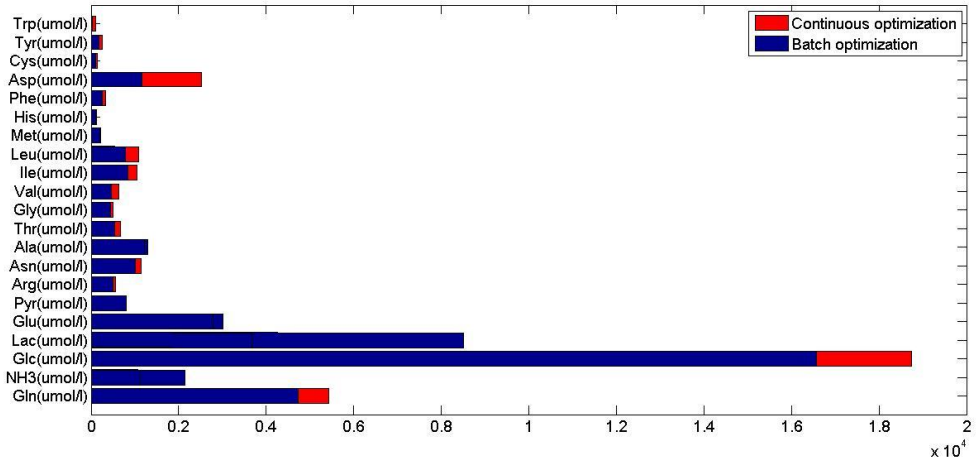

Figure 26. Comparison between the optimal concentrations obtained for the continuous system and the initial optimal concentrations for the batch system.

Comparing the concentrations obtained for both optimizations (Figure 26), in the continuous optimization higher concentrations are used for most compounds and almost no pyruvate is needed, whereas in the batch optimization all compounds are considered. Also in the batch optimization high values of both lactate and ammonia are obtained, in particular in comparison to those obtained experimentally (Table 9), which is not beneficial to the cell and makes this optimization less suitable for being tested.

When comparing the concentrations obtained from both optimizations with the ones used experimentally (average), the continuous optimization stands out again for using much higher concentrations (Table 9), which in this case it is not particularly bad. When trying to optimize a medium that is already defined such as the SMIF8 medium, increasing the concentrations is far easier than decreasing them, so the continuous optimization results is easier to realize than the batch optimization. The only problem will be to eliminate almost completely pyruvate from the SMIF8 medium.

Table 9. Comparison between the average experimental concentrations used in the cultivations and the optimal concentrations obtained for the continuous optimization and batch optimization (µmol/L).

	Experimental concentrations (µmol/L)	Continuous Optimization (µmol/L)	Batch Optimization (µmol/L)
Gln	5252.88	5431.24	4723.38
NH_3	1397.98	1104.58	2137.38
Glc	18774.87	18747.75	16579.10
Lac	6486.61	3670.43	8514.49
Glu	2917.85	2792.12	3020.03
Pyr	861.02	1.11	802.49
Arg	358.08	555.00	499.08
Asn	804.31	1136.41	1002.88
Ala	871.20	1221.08	1295.70
Thr	482.65	665.31	541.72
Gly	334.13	494.00	446.32
Val	532.83	627.29	462.33
Ile	773.02	1039.47	833.36
Leu	794.00	1089.29	785.93
Met	207.46	220.45	198.65
His	124.06	121.72	109.65
Phe	285.06	327.08	255.02
Asp	1425.68	2523.19	1162.85
Cys	146.04	146.60	101.88
Tyr	228.03	247.63	188.62
Trp	62.14	96.18	33.02

Conclusions

MDCK cells have become one of the most used cell lines to produce cell culture-based vaccines, namely against influenza. The growth of mammalian cells to high densities is essential for the development of cost-effective culture processes required in the large-scale production of vaccines. However, reaching such densities still remains a challenge.

A large effort by the scientific community has been made over the last years to develop strategies to yield such densities like for instance medium optimization. Still the conventional methodologies used are time consuming and the associated costs are high.

The medium composition, i.e. the extracellular environment of a cell, has an influence on the cell regulation and therefore on the flux distribution. By understanding the impact of the environment on the cell, different optimization strategies can be proposed towards an increase in cell density.

In this work, a combined methodology was explored in which classical metabolic flux analysis and partial least squares were used to build a regression model between the estimated metabolic state and the cellular environment. The regression model gave a better insight of the role of each component on the flux distribution, namely on the biomass growth rate and enabled the optimization of the medium composition, which was investigated for a batch and a continuous system.

Firstly, the cell metabolism was analyzed based on the experimental concentrations, demonstrating the expected behavior. Significant oscillations were detected for the experimental concentrations of glutamate. This variation affected not only the intracellular and extracellular flux estimation through MFA but also the estimations made by the PLS model, which must be considered during the analysis of the results. Higher biomass growth rates were obtained for the cultivation operated in a wave bioreactor suggesting that this operational system might be better than stirred-tank bioreactors if the purpose is to reach high cell densities, which is in accordance with the literature [15].

Secondly and regarding the MFA, the used metabolic model proved to be valid as most of the fluxes estimated were consistently described. As mentioned before the inaccurate measurements of glutamate led to inconsistent flux estimations. In the case of the reactions involving ATP some inconsistencies were also detected due to the fact that not all ATP-consuming reactions were considered by the metabolic model.

The PLS model captured more than 65% percentage of variance on both dependent and independent variables leading to good predictions of the extracellular and the intracellular fluxes. The model allowed the comprehension of the impact of the environment on the cell's regulation along the time, indicating the possibility of design new optimization strategies which can further improve the cell growth.

Optimization studies with the aim of specific biomass growth rate maximization for concentration manipulations in a batch and continuous system yielded superior growth rate than the ones obtained experimentally. Most of the manipulated concentrations are higher than the ones used experimentally, which makes it easier to manipulate the SMIF8 medium, which is already defined. However, the optimization of the continuous system seems to be more favorable for the following reasons:

1. No pyruvate seems to be needed in the medium composition decreasing the costs of medium production;

2. Higher biomass growth rates are obtained, thus leading to a faster process;

3. Lower levels of lactate and ammonia were estimated by the PLS model, improving the cell growth conditions.

Overall the proposed methodology answered the initial goals of this work. Not only faster processes were obtained but also a better understanding of the role of each component present in the medium. If such methodology based simply on computational simulations is proved to be accurate and exact then medium optimizations for different operational systems can be made for the most varied applications, thus becoming a powerful tool. However, the regulation of the intracellular fluxes cannot be completely unraveled with the proposed approach, i.e. the prediction of the intracellular flux values showed the highest discrepancies.

Future Work

As for future work, the first thing of course should be to test both optimized mediums and see whether the results are the ones expected or not.

It would be also very interesting to include data regarding virus production into our PLS model. It is known that once MDCK cells are infected their metabolism changes. That said, being able to study and manipulate the medium concentration at this stage could result into high virus titers.

The PLS model should be used to study the impact of depleting certain compounds from the medium composition. Having a medium with few components would not only decrease the chance of contaminations but also would reduce the manufacturing costs.

Moreover, the quantification of more metabolites and the addition of more parameters would increase the accuracy of the predictions.

Finally, including different data sets into our PLS model would increase its predictive power leading to more realistic results.

Bibliography

1. Hossain M.J., Perez S., Guo Z., Chen L., Donis R.O.: Establishment and Characterization of a Madin-Darby Canine Kidney Reporter Cell Line for Influenza A Virus Assays. Journal of Clinical Microbiology 2010, 2515–2523.

2. Heldt F.S., Frensing T., Pflugmacher A., Gröpler R., Peschel B., Reichl U.: Multiscale Modeling of Influenza A Virus Infection Supports the Development of Direct-Acting Antivirals. PLoS Comput Biol 2013.

3. Doroshenko A., Halperin S.A.: Trivalent MDCK cell culture-derived influenza vaccine Optaflu® (Novartis Vaccines). Expert Reviews Vaccines 2009, 8(6):679–88.

4. Liu J., Shi X., Schwartz R., Kemble G.: Use of MDCK cells for production of live attenuated influenza vaccine. Elsevier Vaccine 2009, 27(46):6460–6463.

5. Frensing T., Heldt F.S., Pflugmacher A., Behrendt I., Jordan I., Flockerzi D., Genzel Y., Reichl U.: Continuous Influenza Virus Production in Cell Culture Shows a Periodic Accumulation of Defective Interfering Particles. PLoS ONE 2013, 8(9): e72288.

6. Genzel Y., Reichl U.: Continuous cell lines as a production system for influenza vaccines. Expert Reviews Vaccines 2009, 8(12)1681 – 1692.

7. Palache A.M., Brands, R., van Scharrenburg G.J.M.: Immunogenicity and Reactogenicity of Influenza Subunit Vaccines Produced in MDCK Cells or Fertilized Chicken Eggs. The Journal of Infectious Diseases 1997, 176(Suppl 1):S20–3.

8. Paillet C., Forno G., Soldano N., Kratje R., Etcheverrigaray M.: Statistical optimization of influenza H1N1 production from batch cultures of suspension Vero cells (sVero). Elsevier Vaccine 2001, Vaccine 29 7212– 7217.

9. Ritter J.B., Wahl A.S., Freund S., Genzel Y., Reichl U.: Metabolic effects of influenza virus infection in cultured animal cells: Intra- and extracellular metabolite profiling. BMC Systems Biology 2010, 4:61.

10. Youil R., Su Q., Toner T.J., Szymkowiak C., Kwan W-S., Rubin B., Petrukhin L., Kiseleva I., Shaw A.R., DiStefano D.: Comparative study of influenza virus replication in Vero and MDCK cell lines. Journal of Virological Methods 2004, 120:23–31.

11. Genzel Y., Behrendt I., König S., Sann H., Reichl U.: Metabolism of MDCK cells during cell growth and influenza virus production in large-scale microcarrier culture. Elsevier Vaccine 2004, Vaccine 22 2202-2208.

12. Tree J.A., Richardson C., Fooks A.R., Clegg J.C., Looby D.: Comparison of large-scale mammalian cell culture systems with egg culture for the production of influenza virus A vaccine strains. Vaccine 2001, 19(25-26):3444–3450.

13. Schulze-Horsel J., Schulze M., Agalaridis G., Genzel Y., Reichl U.: Infection dynamics and virus-induced apoptosis in cell culture-based influenza vaccine production—Flow cytometry and mathematical modeling. Elsevier Vaccine 2009, 27:2712–2722.

14. Kluge S., Benndorf D., Genzel Y., Scharfenberg K., Rapp E., Reichl U.: Monitoring changes in proteome during stepwise adaptation of a MDCK cell line from adherence to growth in suspension. Elsevier Vaccine 2015.

15. Lohr V., Genzel Y., Behrendt I., Scharfenberg K., Reichl U.: A new MDCK suspension line cultivated in a fully defined medium in stirred-tank and wave bioreactor. Elsevier Vaccine 2010, Vaccine 28(38):6256–6264.

16. Wahl A., Sidorenko Y., Dauner M., Genzel Y., Reichl U.: Metabolic Flux Model for an Anchorage-Dependent MDCK Cell Line: Characteristic Growth Phases and Minimum Substrate Consumption Flux Distribution. Biotechnology and Bioengineering 2008, 101: 135–152.

17. Möhler L., Flockerzi D., Sann H., Reichl U.: Mathematical Model of Influenza A Virus Production in Large-Scale Microcarrier Culture. Biotechnology and Bioengineering 2005, 90, 46–58.

18. Shojaosadati S.A., Kolaei S.M.V., Babaeipour V., Farnoud A.M.: Recent advances in high cell density cultivation for production of recombinant protein. Iranian Journal of Biotechnology 2008, 6(2): 63-84.

19. Frame K.K., Hu W-S.: A Model for Density-Dependent Growth of Anchorage-Dependent Mammalian Cells. Biotechnology and Bioengineering 1988, Vol. 32, Pp. 1061-1066.

20. Bernal V., Carinhas N., Yokomizo A.Y., Carrondo M.J.T., Alves P.M.: Cell Density Effect in the Baculovirus-Insect Cells System: A Quantitative Analysis of Energetic Metabolism. Biotechnology and Bioengineering 2009, 104: 162–180.

21. Genzel Y., Olmer R.M., Schäfer B., Reichl U.: Wave microcarrier cultivation of MDCK cells for influenza virus production in serum containing and serum-free media. Vaccine 2006, 24(35-36):6074–6087.

22. Kong D., Cardak., Chen M., Gentz R., Zhang J.: High cell density and productivity culture of Chinese hamster ovary cells in a fluidized bed bioreactor. Cytotechnology 1999, 29:215–220.

23. Genzel Y., Vogel T., Buck J., Behrendt I., Ramirez D.V., Schiedner G., Jordan I., Reichl U.: High cell density cultivations by alternating tangential flow (ATF) perfusion for influenza A virus production using suspension cells. Elsevier Vaccine 2014, 32:2770–2781.

24. De Alwis D., Dutton R., Scharer J., Moo-Young M.: Statistical methods in media optimization for batch and fed-batch animal cell culture. Bioprocess and Biosystems Engineering 2007, 30: 107–113.

25. Klamt S., Saez-Rodriguez J., Gilles E.D.: Structural and functional analysis of cellular networks with CellNetAnalyzer. BMC Systems Biology 2007, 1:2.

26. Sidorenko Y., Reichl U.: Structured Model of Influenza Virus Replication in MDCK Cells. Biotechnology and Bioengineering 2004, 88: 1–14.

27. De Boor C., Rice J.R.: Least Squares Cubic Spline Approximation I - Fixed Knots. International Mathematical & Statistical Libraries 1968.

28. Cook E.R., Peters K.: The smoothing spline: A new approach to standardizing forest interior tree-ring width series for dendroclimatic studies. Tree-Ring Bulletin 1981, 41:45-53.

29. Scholkmann F., Spichtig S., Muehlemann T., Wolf M.: How to detect and reduce movement artifacts in near-infrared imaging using moving standard deviation and spline interpolation. Physiological Measurement 2010, 31:649–662.

30. Ozturk S.S., Palsson B.O.: Chemical Decomposition of Glutamine in Cell Culture Media: Effect of Media Type, pH, and Serum Concentration. Biotechnology Progress 1990, 6(2):121–128.

31. Schneider M., Marison I.W., von Stockar U.: The importance of ammonia in mammalian cell culture. Journal of Biotechnology 1996, 46(3):161–185.

32. Young K.T., Lee S.Y.: Accurate Metabolic Flux Analysis through Data Reconciliation of Isotope Balance-Based Data. Journal of Microbiology and Biotechnology 2006, 16:1139–1143.

33. Stephanopoulos G.N., Aristou A.A., Nielsen J.: Metabolic engineering: principles and methodologies. Academic Press, San Diego, CA 1998.

34. Zupke C., Sinskey A.J., Stephanopoulos G.: Intracellular flux analysis applied to the effect of dissolved oxygen on hybridomas. Applied Microbiology and Biotechnology 1995, 44:27-36.

35. Bonarius H.P.J., Hatzimanikatis V., Meesters K.P.H., de Gooijer C.D., Schmid G., Tramper J.: Metabolic Flux Analysis of Hybridoma Cells in Different Culture Media Using Mass Balances. Biotechnology and Bioengineering 1996, 50(3):299-318.

36. Varma A., Palsson B.O.: Metabolic Flux Balancing: Basic concepts, scientific and practical use. Nature Biotechnology 1994, 12:994 – 998.

37. Klamt S., Schuster S., Gilles E.D.: Calculability analysis in underdetermined metabolic networks illustrated by a model of the central metabolism in purple nonsulfur bacteria. Biotechnology and Bioengineering 2002, 77:734–771.

38. Miao H., Dykes C., Demeter L.M., Cavenaugh J., Park S.Y., Wu H.: Modeling and Estimation of Kinetic Parameters and Replicative Fitness of HIV-1 from Flow-Cytometry-Based Growth Competition Experiments. Bulletin of Mathematical Biology 2008, 70(6):1749-71.

39. Boulesteix A.L., Strimmer K.: Partial least squares: a versatile tool for the analysis of high-dimensional genomic data. Briefings in Bioinformatics 2007, 8:32–44.

40. Hwang D., Stephanopoulos G., Chan C.: Inverse modeling using multi-block PLS to determine the environmental conditions that provide optimal cellular function. Bioinformatics 2004, 20: 487–499.

41. Wold S., Sjöström M., Eriksson L.: PLS-regression: a basic tool of chemometrics. Chemometrics and Intelligent Laboratory Systems 2001, 58:109–130.

42. Abdi H.: Partial least squares regression and projection on latent structure regression (PLS Regression). Wiley Interdisciplinary Reviews: Computational Statistics 2010, 2:97-106.

43. Von Stosch M., Oliveira R., Peres J., de Azevedo S.F.: A novel identification method for hybrid (N)PLS dynamical systems with application to bioprocesses. Elsevier Expert Systems with Applications 2011, 38:10862–10874.

44. Fonville J.M., Richards S.E., Barton R.H., Boulange C.L., Ebbels T.M.D., Nicholson J.K., Holmes E., Dumas M.E.: The evolution of partial least squares models and related chemometric approaches in metabonomics and metabolic phenotyping. Journal of Chemometrics 2010, 24: 636–649.

45. Rosipal R., Krämer N.: Overview and Recent Advances in Partial Least Squares. New York: Springer-Verlag 2006, 34–51.

46. Ferreira A.R., Dias J.M.L., Teixeira A.P., Carinhas N., Portela R.M.C., Isidro I.A., von Stosch M., Oliveira R.: Projection to latent pathways (PLP): a constrained projection to latent variables (PLS) method for elementary flux modes discrimination. BMC Systems Biology 2011, 5:181.

47. Carinhas N., Bernal V., Teixeira A.P., Carrondo M.J.T., Alves P.M., Oliveira R.: Hybrid metabolic flux analysis: combining stoichiometric and statistical constraints to model the formation of complex recombinant products. BMC Systems Biology 2011, 5:34.

48. Teixeira A.P., Dias J.M.L., Carinhas N., Sousa M., Clemente J.J., e Cunha A., von Stosch M., Alves P.M., Carrondo M.J.T., Oliveira R.: Cell functional enviromics: Unravelling the function of environmental factors. BMC Systems Biology 2011, 5:92.

49. Introduction to Chemometrics and Statistics.

50. Antoniewicz M.R., Stephanopoulos G., Kelleher J.K.: Evaluation of regression models in metabolic physiology: predicting fluxes from isotopic data without knowledge of the pathway. Metabolomics 2006, 2(1): 41–52.

51. Westerhuis J.A., Hoefsloot H.C.J., Smit S., Vis D.J., Smilde A.K., van Velzen E.J.J., van Duijnhoven J.P.M., van Dorsten F.A.: Assessment of PLSDA cross validation. Metabolomics 2008, Volume 4, Issue 1, pp 81-89.

52. Sidorenko Y., Wahl A., Dauner M., Genzel Y., Reichl U.: Comparison of Metabolic Flux Distributions for MDCK Cell Growth in Glutamine- and Pyruvate-Containing Media. Biotechnology Progress 2008, 24(2):311-20.

53. Genzel Y., König S., Reichl U.: Amino acid analysis in mammalian cell culture media containing serum and high glucose concentrations by anion exchange chromatography and integrated pulsed amperometric detection. Analytical Biochemistry 2004, 335(1):119-25.

54. Hassell T., Gleave S., Butler M.: Growth inhibition in animal cell culture: The effect of lactate and ammonia. Appl Biochem Biotechnol 1991, 30(1):29-41.

55. McDermott R.H., Butler M.: Uptake of glutamate, not glutamine synthetase, regulates adaptation of mammalian cells to glutamine-free medium. Journal of Cell Science 1993, 104, 51-58.

Annex

Annex 1

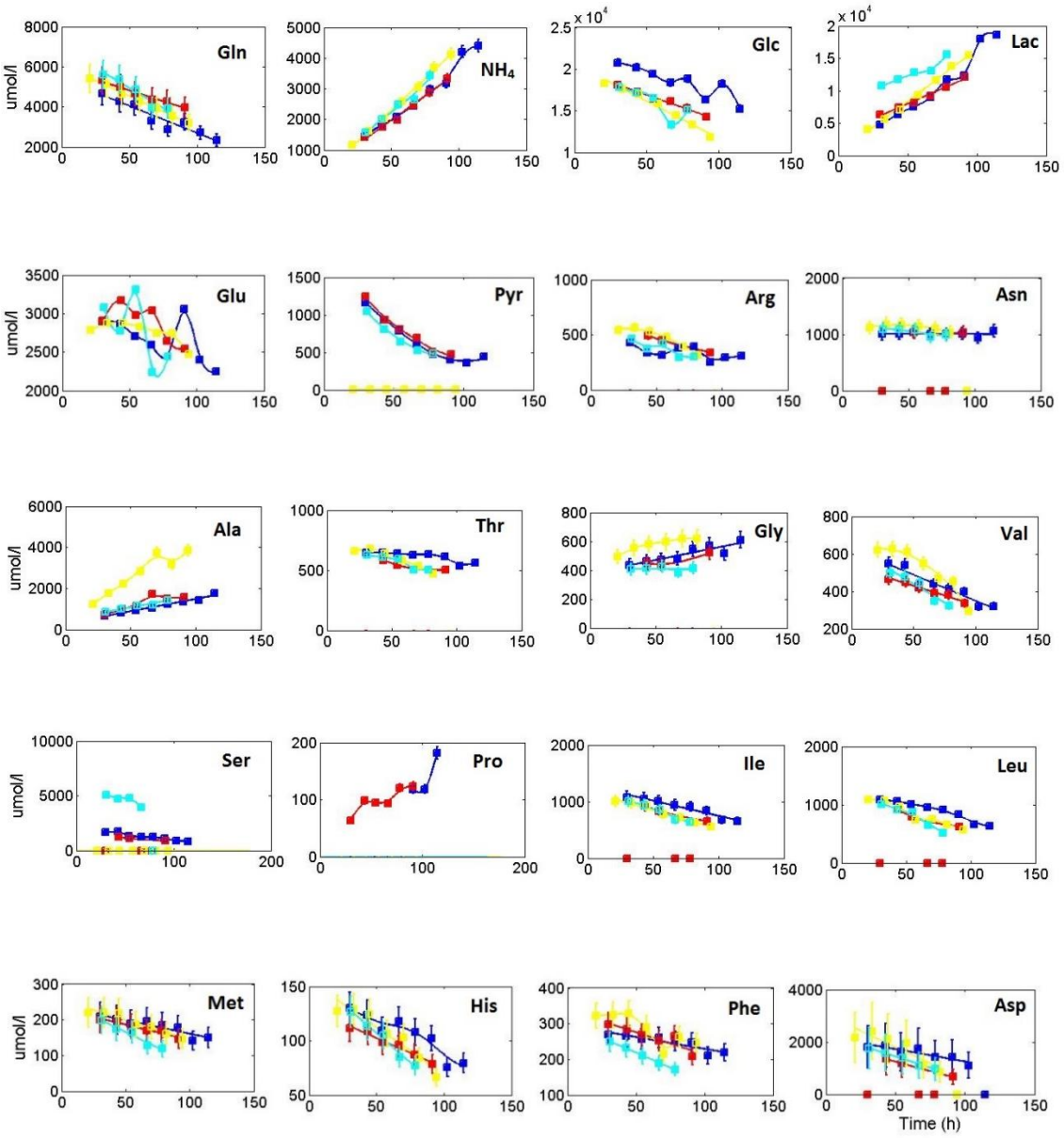

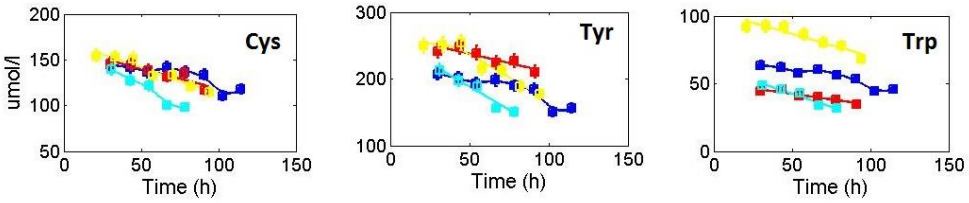

Figure 27. Concentration profiles over time for MDCK suspension cells for all cultivations. The solid lines represent the model fit. The blue line represents the first cultivation, the red line represents the second cultivation, the yellow line represents the third cultivation and the light blue line represents the fourth cultivation.

Annex 2

Table 10 Reactions included on the metabolic model, adapted from Wahl et al [16].

Number		Reaction
1	ENT_GLUC	Glc → Glc_c
2	GLYC_G-6P_F-6P	G-6P_c <==> F-6P_c
3	GLYC_F-6P_GAP	F-6P_c + ATP_c <==> 2 GAP_c
4	PPP_G-6P_R-5P	G-6P_c ==> R-5P_c + CO2_c + 2 NADPH_c
5	GLYC_Pyr_A-CoA	Pyr_m ==> CO2_m + A-CoA_m + NADH_m
6	ANPL_Mal_Pyr_m	Mal_m <==> CO2_m + Pyr_m + NADPH_m
7	TCA_A-CoA&OAA_Cit	A-CoA_m + OAA_m ==> Cit_m
8	TCA_Mal_OAA_m	Mal_m <==> OAA_m + NADH_m
9	TCA_Fum_Mal	Fum_m <==> Mal_m
10	TCA_a-Ket_S-CoA	a-Ket_m ==> S-CoA_m + CO2_m + NADH_m
11	AA_GLU_DS_a-Ket	GLU_m <==> a-Ket_m + NH3_m + NADPH_m
12	AA_GLN_DE_GLU_L649	GLN_c <==> GLU_c + NH3_c
13	GLYC_Lac_Pyr	Pyr_c + NADH_c <==> Lac_c
14	ENT_GLN	0.33 ATP_c ==> GLN_c
15	ENT_GLU	ATP_c ==> GLU_c
16	AA_ALA_DS_Pyr	ALA_c + a-ket_c <==> Pyr_c + GLU_c
17	ENT_ALA	0.33 ATP_c ==> ALA_c

18	AA_ASP_DS_OAA_c	ASP_c + a-ket_c <==> OAA_c + GLU_c
19	ENT_ASP	ATP_c ==> ASP_c
20	mue	mue
21	ENT_NH3	<==> NH3_c
22	ENT_CO2	<==> CO2_c
23	ANPL_Pyr_OAA	CO2_m + Pyr_m + ATP_m ==> OAA_m
24	OTHER_O2&NADH	0.5 O2_c + NADH_m ==> 2.5 ATP_m
25	ENT_O2	==> O2_c
26	ENT_ARG	0.33 ATP_c ==> ARG_c
27	ENT_ASN	0.33 ATP_c ==> ASN_c
28	ENT_CYS	0.33 ATP_c ==> CYS_c
29	ENT_GLY	0.33 ATP_c ==> GLY_c
30	ENT_HIS	0.33 ATP_c ==> HIS_c
31	ENT_ILE	0.33 ATP_c ==> ILE_c
32	ENT_LEU	0.33 ATP_c ==> LEU_c
33	ENT_LYS	0.33 ATP_c ==> LYS_c
34	ENT_VAL	0.33 ATP_c ==> VAL_c
35	ENT_MET	0.33 ATP_c ==> MET_c
36	ENT_PHE	0.33 ATP_c ==> PHE_c
37	ENT_PRO	0.33 ATP_c ==> PRO_c
38	ENT_SER	0.33 ATP_c ==> SER_c
39	ENT_THR	0.33 ATP_c ==> THR_c
40	ENT_TRP	0.33 ATP_c ==> TRP_c
41	ENT_TYR	0.33 ATP_c ==> TYR_c
42	AA_ARG_DE_GLU	ARG_c + a-ket_c <==> NADH_c + Urea_c + 2 GLU_c
43	AA_ASN_ASP_DS_L653	ASN_c <==> ASP_c + NH3_c

44	AA_HIS_DE_GLU	HIS_c ==> NADH_c + CO2_c + GLU_c + NH3_c
45	AA_ILE_DE_A-CoA	ILE_c + ATP_m + a-ket_c ==> S-CoA_m + A-CoA_m + NADH_m + FADH2_m + GLU_c
46	AA_LEU_DE_A-CoA	LEU_c + ATP_m + a-ket_c ==> 3 A-CoA_m + FADH2_m + GLU_c
47	AA_LYS_DE_A-CoA	LYS_c + NADPH_c + 2 a-ket_c ==> 2 CO2_m + 2 A-CoA_m + 2 NADH_c + 2 NADH_m + FADH2_m + 2 GLU_c
48	AA_MET_DE_FUM	MET_c + SER_c + 3 ATP_c + ATP_m ==> S-CoA_m + CYS_c + NADH_m + CO2_c + NH3_c
49	AA_PHE_DE_FUM	O2_c + PHE_c + NADPH_c ==> TYR_c
50	AA_PRO_DE_GLU	PRO_c <==> 2 NADH_c + GLU_c
51	AA_THR_DE_GLY	THR_c ==> CO2_m + NADH_c + Pyr_m + NADH_m + FADH2_m + NH3_c
52	AA_TRP_DE_A-CoA	3 O2_c + TRP_c + NADPH_c ==> ALA_c + 2 CO2_m + 2 A-CoA_m + 2 NADH_m + 2 CO2_c + FADH2_m + NH3_c
53	AA_VAL_DE_FUM	VAL_c + a-ket_c ==> S-CoA_m + 2 NADH_m + CO2_c + FADH2_m + GLU_c
54	AA_TYR_DE_A-CoA_&_FUM	2 O2_c + TYR_c + a-ket_c ==> Fum_c + 2 A-CoA_m + CO2_c + GLU_c
55	GLYC_GAP_PGA	GAP_c <==> NADH_c + ATP_c + PGA_c
56	GLYC_PGA_PEP	PGA_c <==> PEP_c
57	GLYC_PEP_Pyr	PEP_c ==> Pyr_c + ATP_c
58	TRANS_Pyr_c_m	Pyr_c <==> Pyr_m
59	TRANS_a-ket_m_c	a-Ket_m <==> a-ket_c
60	PPP_R-5P_F-6P&GAP	R-5P_c + E-4P_c <==> F-6P_c + GAP_c
61	PPP_R-5P_GAP	2 R-5P_c <==> GAP_c + S-7P_c
62	PPP_GAP_F-6P	GAP_c + S-7P_c <==> F-6P_c + E-4P_c
63	ENT_Pyr	0.33 ATP_c ==> Pyr_c
64	OUT_ATP	ATP_c ==>

65	ENT_Gal	==> Gal_c
66	GLYC_Glc_G-6P	ATP_c + Glc_c ==> G-6P_c
67	GLYC_Gal_G-6P	ATP_c + Gal_c ==> G-6P_c
68	ANPL_Mal_Pyr_c	Mal_c <==> Pyr_c + CO2_c + NADPH_c
69	ANPL_OAA_PEP	ATP_c + OAA_c <==> PEP_c + CO2_c
70	TRANS_CO2_c_m	CO2_c <==> CO2_m
71	TCA_Cit_a-ket	Cit_m <==> a-Ket_m + CO2_m + NADH_m
72	TCA_Mal_OAA_c	Mal_c <==> NADH_c + OAA_c
73	TRANS_Cit_Mal_m_c	Mal_c + Cit_m <==> Mal_m + Cit_c
74	TCA_Cit_A-CoA&OAA	ATP_c + Cit_c ==> OAA_c + A-CoA_c
75	OTHER_O2&FADH2	0.5 O2_c + FADH2_m ==> 1.5 ATP_m
76	TRANS_ATP_m_c	ATP_m <==> ATP_c
77	AA_GLY_DS_SER	2 GLY_m <==> CO2_m + NH3_m + SER_m + NADH_m
78	AA_SER_DE_Pyr	SER_c <==> Pyr_c + NH3_c
79	OTHER_NADH_NADPH	NADH_m <==> NADPH_m
80	AA_CYS_DE_PYR	O2_c + CYS_c + a-ket_c ==> Pyr_c + GLU_c
81	OUT_Urea	Urea_c <==>
82	TRANS_GLU_c_m	GLU_c <==> GLU_m
83	TRANS_ASP_GLU_m_c	GLU_c + ASP_m <==> ASP_c + GLU_m
84	TRANS_NH3_c_m	NH3_c <==> NH3_m
85	AA_ASP_DS_OAA_m	a-Ket_m + ASP_m <==> GLU_m + OAA_m
86	TRANS_Mal_c_m	Mal_m <==> Mal_c
87	Lip_CH_synt	8 O2_c + 18 ATP_c + 18 A-CoA_c + 20 NADPH_c ==> 9 CO2_c + CH
88	Lip_PC_synt	GAP_c + SER_c + 6 ATP_c + 2 CO2_c + A-CoA_c + NADPH_c ==> PC

89	Lip_PE_synt	GAP_c + SER_c + 3 ATP_c + A-CoA_c + NADPH_c ==> CO2_c + PE
90	Lip_PS_synt	GAP_c + SER_c + 3 ATP_c + A-CoA_c + NADPH_c ==> PS
91	Lip_PG_synt	2 GAP_c + 17.6 ATP_c + 17.6 A-CoA_c + 31.7 NADPH_c ==> PG
92	Lip_PI_synt	G-6P_c + GAP_c + 17.6 ATP_c + 17.6 A-CoA_c + 30.7 NADPH_c ==> PI
93	Lip_SM_synt	3.1 SER_c + 10.2 ATP_c + 1.7 NADPH_c ==> FADH2_m + SM
94	vLip_CH_synt	8 O2_c + 18 ATP_c + 18 A-CoA_c + 20 NADPH_c ==> 9 CO2_c + vCH
95	vLip_PC_synt	GAP_c + SER_c + 6 ATP_c + 2 CO2_c + A-CoA_c + NADPH_c ==> vPC
96	vLip_PE_synt	GAP_c + SER_c + 3 ATP_c + A-CoA_c + NADPH_c ==> CO2_c + vPE
97	vLip_PS_synt	GAP_c + SER_c + 3 ATP_c + A-CoA_c + NADPH_c ==> vPS
98	vLip_PG_synt	2 GAP_c + 17.6 ATP_c + 17.6 A-CoA_c + 31.7 NADPH_c ==> vPG
99	vLip_PI_synt	G-6P_c + GAP_c + 17.6 ATP_c + 17.6 A-CoA_c + 30.7 NADPH_c ==> vPI
100	vLip_SM_synt	3.1 SER_c + 10.2 ATP_c + 1.7 NADPH_c ==> FADH2_m + vSM
101	TCA_Fum_Mal_c	Fum_c <==> Mal_c
102	TRANS_GLY_c_m	GLY_c <==> GLY_m
103	TRANS_SER_c_m	SER_c <==> SER_m
104	TCA_S-CoA_Fum	S-CoA_m <==> Fum_m + ATP_m + FADH2_m
105	ENT_Lac	<==> Lac_c
106	OUT_CYS	CYS_c ==>
107	OUT_GLY	GLY_c ==>

108	OUT_ASP	ASP_c ==>
109	OUT_ASN	ASN_c ==>
110	OUT_GLU	GLU_c ==>
111	OUT_GLN	GLN_c ==>
112	OUT_ALA	ALA_c ==>
113	OUT_TYR	TYR_c ==>
114	OUT_ARG	ARG_c ==>
115	OUT_SER	SER_c ==>
116	OUT_PRO	PRO_c ==>
117	OUT_CH	CH ==>
118	GLX_ICL	Cit_m ==> Fum_m + Glx_m
119	GLX_MS	A-CoA_m + Glx_m ==> Mal_m
120	SYNT_PB2	PB2 ==> 31 ASP_c + 44 ALA_c + 36 GLN_c + 61 ARG_c + 34 ASN_c + 5 CYS_c + 49 GLY_c + 10 HIS_c + 52 ILE_c + 59 LEU_c + 45 LYS_c + 61 VAL_c + 37 MET_c + 25 PHE_c + 29 PRO_c + 52 SER_c + 51 THR_c + 10 TRP_c + 16 TYR_c + 3268.25 ATP_c + 52 GLU_c
121	SYNT_PB1	PB1 ==> 31 ASP_c + 41 ALA_c + 31 GLN_c + 53 ARG_c + 49 ASN_c + 10 CYS_c + 47 GLY_c + 10 HIS_c + 46 ILE_c + 57 LEU_c + 50 LYS_c + 33 VAL_c + 40 MET_c + 33 PHE_c + 32 PRO_c + 50 SER_c + 61 THR_c + 9 TRP_c + 25 TYR_c + 3259.64 ATP_c + 49 GLU_c
122	SYNT_PA	PA ==> 36 ASP_c + 37 ALA_c + 19 GLN_c + 40 ARG_c + 34 ASN_c + 15 CYS_c + 36 GLY_c + 13 HIS_c + 48 ILE_c + 65 LEU_c + 53 LYS_c + 30 VAL_c + 25 MET_c + 36 PHE_c + 31 PRO_c + 52 SER_c + 37 THR_c + 12 TRP_c + 20 TYR_c + 3083.1 ATP_c + 77 GLU_c
123	SYNT_HA	HA ==> 21 ASP_c + 33 ALA_c + 17 GLN_c + 21 ARG_c + 49 ASN_c + 16 CYS_c + 42 GLY_c + 13 HIS_c + 36 ILE_c + 51 LEU_c + 38 LYS_c + 33 VAL_c + 10 MET_c + 19 PHE_c + 20 PRO_c + 46 SER_c + 28 THR_c + 10 TRP_c + 25 TYR_c + 2437.2 ATP_c + 38 GLU_c

124	SYNT_NP	NP ==> 23 ASP_c + 39 ALA_c + 21 GLN_c + 49 ARG_c + 25 ASN_c + 6 CYS_c + 41 GLY_c + 6 HIS_c + 26 ILE_c + 32 LEU_c + 21 LYS_c + 24 VAL_c + 25 MET_c + 18 PHE_c + 17 PRO_c + 39 SER_c + 29 THR_c + 6 TRP_c + 15 TYR_c + 2144.39 ATP_c + 36 GLU_c
125	SYNT_NA	NA ==> 25 ASP_c + 16 ALA_c + 11 GLN_c + 20 ARG_c + 25 ASN_c + 19 CYS_c + 44 GLY_c + 10 HIS_c + 41 ILE_c + 21 LEU_c + 23 LYS_c + 28 VAL_c + 7 MET_c + 16 PHE_c + 21 PRO_c + 51 SER_c + 29 THR_c + 16 TRP_c + 14 TYR_c + 1954.92 ATP_c + 17 GLU_c
126	SYNT_NS1	NS1 ==> 15 ASP_c + 16 ALA_c + 8 GLN_c + 20 ARG_c + 8 ASN_c + 2 CYS_c + 14 GLY_c + 2 HIS_c + 14 ILE_c + 24 LEU_c + 12 LYS_c + 15 VAL_c + 9 MET_c + 7 PHE_c + 11 PRO_c + 16 SER_c + 14 THR_c + 4 TRP_c + TYR_c + 990.38 ATP_c + 18 GLU_c
127	SYNT_NEP	NEP ==> 5 ASP_c + 2 ALA_c + 10 GLN_c + 8 ARG_c + 5 ASN_c + 5 GLY_c + 3 HIS_c + 8 ILE_c + 17 LEU_c + 6 LYS_c + 4 VAL_c + 7 MET_c + 7 PHE_c + PRO_c + 11 SER_c + 5 THR_c + 2 TRP_c + TYR_c + 521 ATP_c + 14 GLU_c
128	SYNT_M1	M1 ==> 6 ASP_c + 25 ALA_c + 15 GLN_c + 17 ARG_c + 11 ASN_c + 3 CYS_c + 16 GLY_c + 5 HIS_c + 11 ILE_c + 26 LEU_c + 13 LYS_c + 16 VAL_c + 14 MET_c + 7 PHE_c + 8 PRO_c + 18 SER_c + 18 THR_c + TRP_c + 5 TYR_c + 1085.11 ATP_c + 17 GLU_c
129	SYNT_M2	M2 ==> 5 ASP_c + 5 ALA_c + 2 GLN_c + 7 ARG_c + 3 ASN_c + 3 CYS_c + 8 GLY_c + 2 HIS_c + 8 ILE_c + 10 LEU_c + 5 LYS_c + 4 VAL_c + 2 MET_c + 4 PHE_c + 4 PRO_c + 7 SER_c + 4 THR_c + 2 TRP_c + 3 TYR_c + 417.682 ATP_c + 9 GLU_c